Addis Ababa University

Graduate Programs

Department of Physics

Visualizing Electromagnetic Vacuum by MRI

BY

BERHANU KELBISO

A thesis submitted to Graduate programs of Addis Ababa University in partial fulfillment of the requirements for the degree of Master of Science in Physics (Imaging Physics)

ADVISER: TESFAYE KIDANE (Ph. D)

November, 2017

Addis Ababa, Ethiopia

Visualizing Electromagnetic (EM) Vacuum by MRI

BY:

BERHANU KELBISO

A THESIS SUBMITTED TO GRADUATE PROGRAMS ADDIS ABABA UNIVERSITY IN PARTIAL FULFILLMENT OF THE REQUIREMENTS FOR THE DEGREE OF MASTER OF SCIENCE IN PHYSICS (IMAGING PHYSICS)

ADVISER: TESFAYE. KIDANE (Ph.D)

November, 2017

ADDIS ABABA, ETHIOPI

ADDIS ABABA UNIVERSITY

COLLAGE OF NATURAL AND COMPUTATIONAL SCIENCE

GRADUATE PROGRAMS

This is to certify the thesis prepared by **BERHANU KELBISO** entitled of **''Visualizing Electromagnetic Vacuum by MRI''** submitted in partial fulfillment of the requirements for the degree of **Master of Science in Physics (Imaging Physics).** Compiles with the regulations of the university and meets the accepted standards with respect to originality.

Signed by the Examining committee:

Adviser: Tesfaye Kidane(Ph.D) Signature: __________ Date: ____________

Examiner: Teshome Senbeta(Ph.D) Signature: __________ Date: ____________

Examiner: Mulugeta Bekele(Ph.D) Signature: ___________ Date: ____________

November, 2017

Addis Ababa University

Addis Ababa Ethiopia

ADDIS ABABA UNIVERSITY

AUTHOR: BERHANU KELBISO

TITLE: **Visualizing Electromagnetic Vacuum by MRI**

Department: PHYSICS

Degree: M.Sc.

Convocation: November Year: 2017

DEDICATION

This Work is dedicated to:

My Father: KELBISO MEKEBO

And

My mother: AMERACH GINTAMO

Table of Content

Abstract

Based upon Maxwell's equations, it has long been established that oscillating EM fields due to current carrying wire incident upon a metal surface, decay exponentially inside the conductor and this leads to the absence of EM fields at sufficient depths. Magnetic resonance imaging (MRI) utilizes radiofrequency (r.f.) EM fields to produce images. Here the first visualization of a virtual EM vacuum inside a bulk metal strip by MRI has been discussed and reviewed using the basic principle of RF EM field in MRI physics. This work is based on radio frequency field calculation inside cylindrical shell of finite thickness and infinite length due to excitation by concentric coils placed inside the shell. The B_1 field calculation is made analytically using mathematical methods of separation of variable and the result is shown in terms of modified Bessel function and the skin depth effect and the result is simulated. Finally B_1 field is the key component in MRI system and it also determines the EM vacuum in the case of low signal.

Acknowledgements

First, I would like to thank the GOD who made everything in this world possible, and He who helped me to begin and finish this work successfully as it is expected.

Next, I would like to extend my heartfelt thanks to my advisor Dr.Tesfaye. Kidane I do not have adequate words to express my feelings of gratitude for his generous guidance and constant encouragement that helped me to complete the present research work successfully. He is the person who has always helped me. His constant encouragement made me strong enough to face every difficulty with confidence during this research study.

I would like to offer my special thanks to Hadiya Zone Mirab Badewecho Woreda Education Office for allowing me sponsorship to attend my post graduate studies.

I am also grateful to acknowledge Addis Ababa University Collage of Natural and computational Science and department Physics for giving an opportunity and access to study my master's degree (MSc).

The last, but not least I would like to give special and precious thanks to my beloved families for their heart full and encouragement through the time and giving constructive comments during my work.

List of Figures

List of tables

ACRONYMS

Symbol	**Description**
MRI	Magnetic Resonance Imaging
NMR	Nuclear Magnetic Resonance
RF	Radio Frequency
T_1	Spin-Lattice Relaxation Time (longitudinal relaxation time)
T_2	Spin –Spin Relaxation Time (transverse relaxation time)
CT	Computer Tomography
PET	Positron Emission Tomography
SPECT	Single Photon Emission Computed Tomography
B_O	Main Magnetic Field
SNR	Signal-to-Noise Ratio
$\hbar$	Planck ’s Constant
γ	Gyro Magnetic Ratio
$\vec{I}$	Spin Angular momentum
m	Potential Quantum States
E_m	Potential Energy States
M_o	Magnetization
K	Boltzmann’s Constant
T	Temperature
ρ	Proton Density
ω_O	Larmor Frequency
v	Velocity of Particle

v_α	Actual Velocity
J	Current Distribution
μ_o	Permeability of Free Space
μ_r	Relative Permeability
ξ	Electromagnetic Field
emf	Electromotive Force
Φ	Magnetic Flux
δ	Skin Depth
δ_{eff}	Effective Subsurface Depth
ε_r	Relative Permittivity
J_C	Conduction Current Density
J_D	Displacement Current Density

Chapter one

1. Background

MRI is an essential measurement and diagnostic tool in medical and non-medical fields. In1946, F.Bloch [1] and Edward Purcell [2] independently described that they could manipulate the residual magnetization of spin that are placed in a magnetic field by irradiating at frequency corresponding to the energy difference (Larmor frequency) between the high and low energy proton spin states. In conjunction with an earlier discovery by Sir Joseph Larmor, they saw that small electromagnetic currents were induced in a nearby RF coil, which corresponded to the angular frequency of precession of the nuclei about the field and was subsequently named NMR. In the following years NMR spectroscopy was then developed and used for chemical analysis and in 1974 [3] Paul C. Lauterbur described the use of Nuclear Magnetic Resonance to form an image of a sample. The first clinical MR systems were installed in 1983 at low field strengths of 0.35-0.5 T [4] followed by the development of 1 T and 1.5 T magnets. Over the past 25 years, these two have been the main field strengths in clinical settings. Over the last 10 years, 3 T MR Scanners were introduced as a clinical modality.

In 1937, [5] NMR phenomenon in molecular beams: RF energy is absorbed by atomic nuclei within samples placed in a strong magnetic field. For the absorption to be efficient the RF must have a special frequency called resonance frequency or Larmor frequency. The Larmor frequency is defined by the magnetic field strength and the atomic nuclei.

EM field of all frequencies represent one of the most common environmental influences, and EM field exposure levels of the population will continue to increase with technological advances. Since the 1960s, anxiety and speculation has grown among the public about the consequence of casual exposure to or continuous interaction with different sources of EM field emission [6]. The EM environment consists of natural radiation and man made EM fields that are produced either intentionally or as by-products of the use of electrical devices and systems. Based on this, all populations are now exposed to varying degrees of EM fields, and the levels will continue to increase as technology advances.

1.1 Introduction

MRI is a Magnetic Resonance medical imaging technique that is the most commonly used in radiology to visualize detailed internal organs, structures, and tissues of the human body based on nuclear resonance of atoms within the body. MRI is significantly more sensitive to the presence of hydrogen, one of the most abundant components in human organs. In addition, hydrogen which consists of a single proton has a relatively large magnetic moment and finally, the human body is composed of tissues that contain primarily water and fat, both of which contain hydrogen. For these reasons, MRI uses hydrogen protons as a source for MRI signals. MRI it utilizes three types of magnetic field coils (main, gradient and RF) to accomplish the harmless imaging procedure. It also provides more information than other imaging modality, since MRI signals depend on several tissue parameters. Contrast in MRI depends not only on the hydrogen density, but also on the additional properties of the sample described by the T_1 and T_2 relaxation time constants (which will be discussed in next topic). These constants can be exploited to yield high quality images.

MRI is a powerful non-invasive and relatively safe imaging technique as compared to other imaging techniques like X-rays, CT, PET and SPECT which makes use of harmful ionizing radiations. While all the image modality is limited to axial plane, MRI can capture images in axial, coronal as well as sagittal plane without moving the patient. Thus, MRI is intrinsically a 3D imaging technique. In addition to anatomical information, MRI images convey useful information regarding organ function and metabolic activities. MRI has also become preferred method for examination of brain and spinal cord with indications including suspected tumors, slipped disks, multiple sclerosis and degenerative diseases. It is widely applied for orthopedics and musculoskeletal imaging.

A typical clinical MRI system is shown in Figure 1.1 below. The major external components are utilized by the patient and technician, which are the magnet bore, patient table and external controls. The magnet bore is the large access in the center of the MRI system. The patient lies on a patient table which will slide into the magnet controlled by a technician operating the controls located on the exterior of the machine.

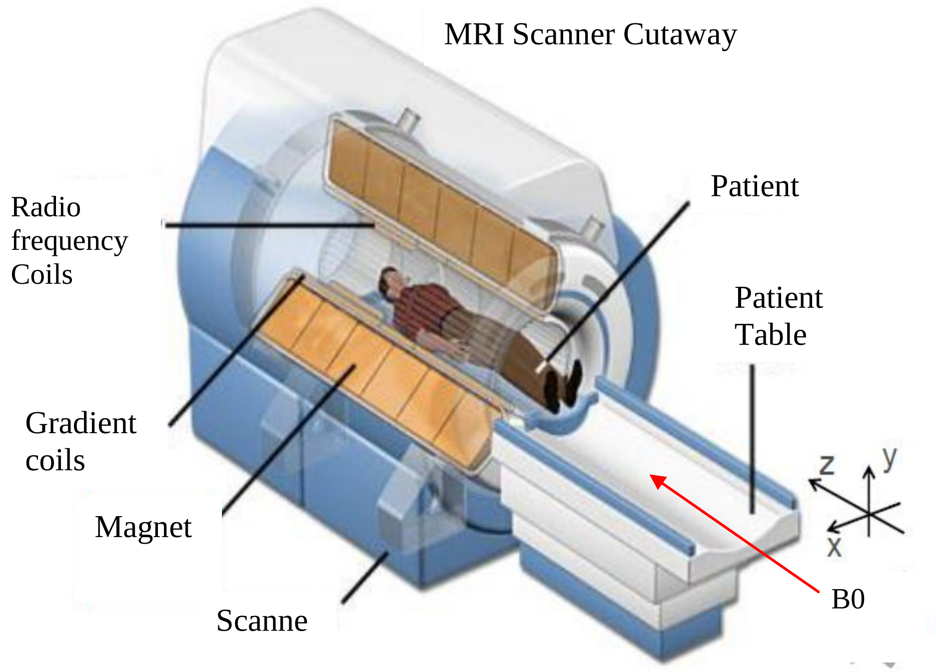

Figure 1.1 MRI machines [7]

The MRI scanner includes the following hardware components of which the main magnet is the most impressive. This powerful magnet creates a B_0 field which is pointing in the direction of the MR bore, by convention taken as the z-direction.

The following sections will explore more in explain the functions of the main magnet, gradient coil system, RF coils and RF amplifiers.

- **The main magnet** is the source of the static magnetic field known as the Bo field. The magnet is the main and the most expensive part of the MRI system. The main Magnets are usually categorized as low, medium, or high-field systems. Low-field magnets have main field strengths less than 0.5 T. Medium-field systems have main magnetic fields between 0.5 and 1T, high-field systems have fields between 1 T and 1.5 T , and ultra-high-field systems have fields of 3T or (≥ 3). It also produces a static magnetic field $B = B_0\hat{z}$ to cause a population of spins to align parallel to the field resulting in the net magnetization which will be manipulated to produce an MRI signal. Since the MRI signal is proportional to the main magnetic field strength.
- **Gradient Coil is** an important part of MRI that provided spatial encoding to the nuclear magnetic resonance signals emitted from magnetized hydrogen protons in human tissues. They also play an important role in determining how fast and accurately an image is obtained. In order to provide spatial

information from the MRI signal, as well as to control the active imaging slice, the Bo field is modified through a spatial gradient field. This means that the magnetic field in the bore of the magnet will only be equal to Bo for a small length along a given axis within the bore. The MRI system uses a set of three orthogonal gradient coils, one for each axis known as the G_x, G_y and G_z coils, thus spatial gradients of the main magnetic field may be applied in the x, y, and z axes within the bore of the MRI magnet.

- **RF coil** is an essential element in MRI systems and therefore its correct design is important. RF coils are the coil of the MRI system that broadcasts the RF signal to the patient or receives the return signal. RF coil has the following purposes in MRI.
- **RF Transmit Coil,** this coil, traditionally a volume coil that is most often built into the main magnet bore of the MRI system, is used for the transmission of RF energy into the body. The frequency of this RF pulse is determined by the Larmor equations, so that the energy in the RF pulse can be absorbed by the spinning nuclei and thus alters their alignments. When the RF pulse is turned off, the atoms will begin to return to their aligned state with the main magnetic field. As these nuclei return to their originally aligned state, they emit energy, which can be received as an induced voltage signal by the RF receive coil. The induced coil voltage forms the basis of this MRI signal.
- **RF Receive Coil,** this coil is to receive the signals from the excited spins and the coils which perform this function are referred to as the receive coils. After the energy has been transmitted and absorbed by the nuclei of the subject, the nuclei will begin to re-align itself with the main magnetic field. As they do, they emit energy at the same Larmor frequency, and the time varying flux induces a voltage in the RF receive coil. There are two general types of RF receiving coils, volume and surface coils. Volume coils have coil element configurations with long conductors spaced around a cylindrical structure. They are known for their extremely high field homogeneity, because of their size, they do not have Signal to Noise Ratio (SNR) as a typical surface coil given the same imaging in the region of interest (ROI). Surface coils on the other hand, are known for their typically high SNR, but lower field homogeneity and field of view than a volume coil. [8]

- **RF Power Amplifiers** are required to produce an RF signal used to modify the alignment of the nuclei being imaged. The amplifiers power the RF transmit coil in order to produce a strong homogenous B_1 field. The view of an MRI system is shown in Figure 1.2.below**.**

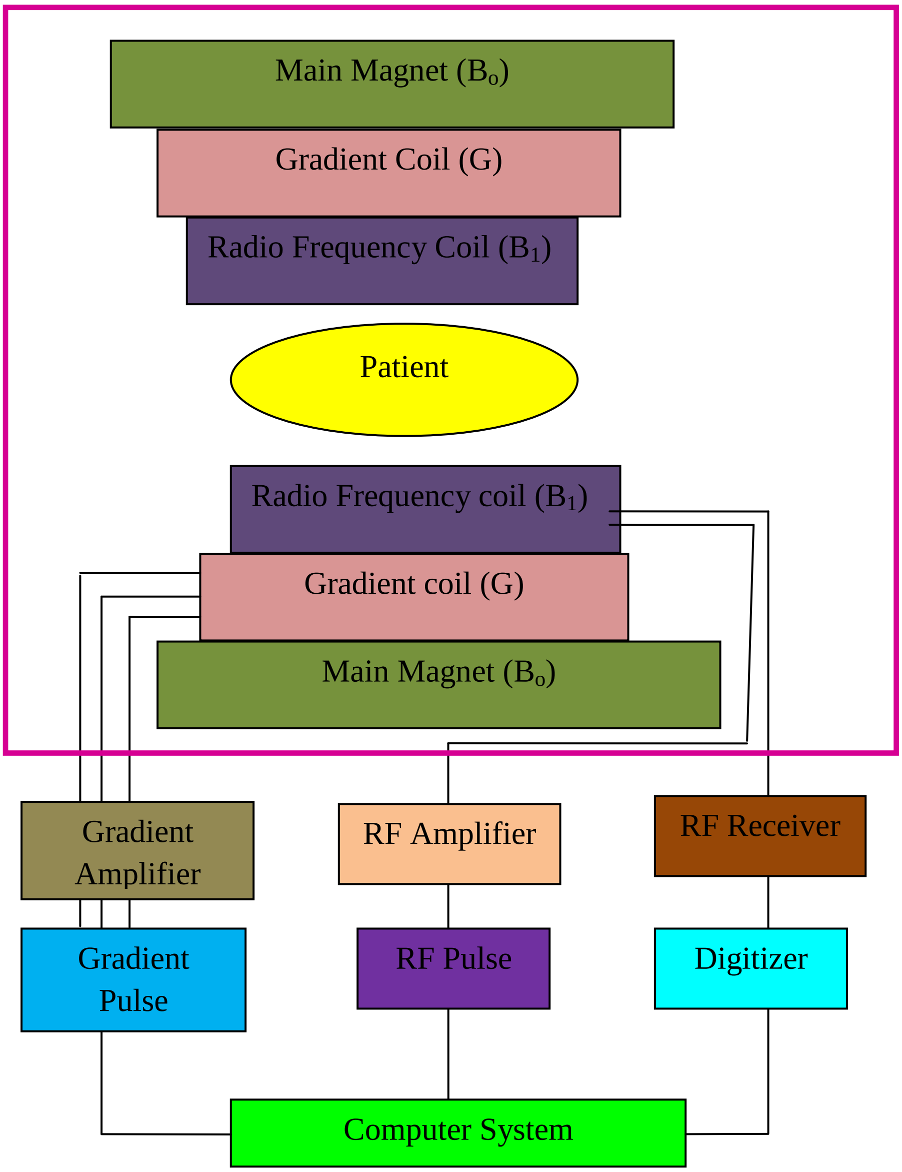

Figure 1.2: MRI System Block Diagram [9]

We know that MRI system typically utilizes three magnetic fields to polarize, encode, and detect nuclear spins. These specific magnetic fields are produced by corresponding coils, which are the main magnet, gradient and both transmit and receive systems, respectively. The main magnet provides a strong, temporal stable, uniform magnetic field to polarize all the spins is subject to the thermal fluctuation, after which the RF transmit system generates a high-frequency field corresponding to the Larmor frequency in order to tip spins to transverse plane for detection. Mean while, a gradient system is applied to encode the spatial information into the MRI signal for detection and a receiver coil is used to pick up all the signals from the sample. For all of this, computer software is crucial for controlling all the pulse sequences, data collection and image reconstruction.

In MRI, patients with metallic implants or an image-guided performed with a metallic needle; one is evidently required to perform MRI in the presence of metal. At the magnetic fields of 1.5 T and above used in clinical MRI scanners, metallic objects can not only be a safety hazard [10] for the patient but can produce artifacts in the resonant image [11]. There are two sources of artifacts: susceptibility differences between the metal and the surrounding tissue, and RF screening by the metal.

Susceptibility artifacts arise from local B_0 field in homogeneities caused by discontinuities in magnetic susceptibility at the boundaries of the metallic material is characterized by geometric distortions in the readout direction of the image, perturbation in the selected slice and signal intensity variations. The severity of the artifact depends on the metallic object geometry, orientation with respect to the static field, the magnetic susceptibility difference, and the strength of the B_0 field [12]. The susceptibility difference between the metal and the surrounding material causes a local magnetic field in homogeneity which is proportional to the measurement field $B_{0.}$

Switched magnetic field gradients and RF pulses can induce eddy currents in a metallic object, which may result in image distortion and image artifacts [13]. In each case the varying field alters the magnetic flux through the conductive object and induces eddy currents due to Faraday's law. Lenz's law states that the eddy current flows so as to oppose the flux change inside the current path. RF eddy currents induced in the metallic object can result in B_1 enhancement or cancellation near the surface of the Object [14]. B_1 homogeneity in the sample space can be significantly altered. Due to the principle of reciprocity, any variation in the B_1 field has an effect both on signal excitation and signal detection. The time varying B_1 field caused by eddy currents is superimposed upon the originally applied B_1 field [15]. B_1 fields are critical to nuclear excitation and signal reception in MRI. Wave propagation of the RF field induced EM field as described in Maxwell's equation [16]. B_1 simulations are used for a wide variety of purposes in MRI today. Historically, they have been used to explain observed phenomena, predict and explore future trends, and ensure RF safety.

In this study B_1field orientation has been under taken to the calculate B_1 field in the sample space surrounding metal conductor and we can try to see the EM vacuum inside in a cylindrical shell by calculating MRI signal. We also analytically calculate the B_1 field in the sample space with introduced MRI coil. The oscillating electromagnetic (EM) field's incident upon a metal surface decay exponentially inside the conductor, this leads to a virtual EM vacuum at sufficient depths. Therefore, B_1 field are the key components in MRI systems and also determine the EM vacuum in the case of low signal.

1.2 Motivation and Objective

MRI is one of the most widely used medical imaging techniques to produce high quality images of the inside of the human body. This unique imaging method is noninvasive and requires no radioactivity.

Radiofrequency magnetic fields are critical to nuclear excitation and signal reception in magnetic resonance imaging. The interactions between these fields and human tissues in anatomical geometries results in a variety of effects regarding image integrity and safety of the human body.

The standard skin depth model for the penetration of EM field in to conductor is reviewed and extended to cover dielectric materials. Skin depth is a distance to which all components of the EM field has in intensity by a factor of e is valid. Another complicating factor acquiring MRI signal of bulk metal is the strong signal dependence on the orientation between the sample and the RF field.

An unanticipated difficulty with MRI and in addition to the skin depth effects was that the orientation of the given material with respect to the RF coil had a significant influence on the quality and the appearance of the image. It was found that the metal object had to be oriented in parallel to the RF field direction for optimal RF excitation of the MRI signal. By contrast, a perpendicular arrangement resulted in a minimum of penetration. This effect is known in the context of EM wave propagation at the interface between a dielectric and a conducting surface.

The RF fields with the conducting cylindrical shell of finite thickness and infinite length can be calculated by analytical solution of field due to excitation current testing problem in cylindrical coordinates is obtained in the case of excitation coil of the probe is coaxially situated inside cylindrical tube whose magnetic permeability depends on the radial coordinate.

Visualizing EM vacuum used in MRI, we are consider with the z-component of the B_0 field and B_1 field. Furthermore, we are considering the radial aligned cylindrical shell of metallic conductor.

All analytic calculation of B_1 field forms involved in the evaluation of the skin depth effect and subsequent construction of magnetic fields are given in terms of exponential and modified Bessel functions.

1.3 Principle of MRI Physics

Radio wave are low energy EM wave and fall in the same range of those used for radio, TV broadcasts and other communication system. MRI uses these radio waves to create image, which have a much lower energy than other EM spectrum. When energy in the form of EM wave is directed at a substance at a particular frequency, the energy is absorbed by the tissue and emitted back a signal can be detected and recorded.

1.3.1 Spins in magnetic resonance Imaging

Spin in MRI is an essential property of nature like electrical charge or mass. Spins come in multiples of 1/2 and has positive or negative values. All protons, neutrons, and electrons in an atom possess the property of spin. Different unpaired protons, neutrons, and electrons have a spin of 1/2. If we consider an atom of deuterium (H^2), it has one each of an unpaired neutron and an unpaired electron. Hence, its total electronic spin will be 1/2, and its total nuclear spin will be 1. Multiple particles having opposite signs of spins tend to pair together in order to avoid the observable appearances of spin, as seen in helium. Different types of nuclei have distinct spin values. Proton ^1H has a spin $\hbar = \dfrac{h}{2\pi}$ where $\hbar$ is the Planck's constant. When a particle is placed in a magnetic field with strength B_0 its net spin will absorb a photon of frequency ω, and it depends on γ which is the particle's gyro magnetic ratio. The equation used to find this frequency is known as the Larmor Equation and is defined as:

$$\omega = \gamma B_O, \tag{1.1}$$

where ω is the RF frequency in MHz, B_0 is the strength of the main magnetic field in Tesla, and γ is the gyro magnetic ratio (γ = 42.6 MHz/T). Table 1.3 lists the most common types of nuclei used in MRI.

Nucleus	Gyro magnetic Ratio (MHz)/T γ
^{1}H	42.6
^{19}F	40.2
^{31}P	11.2
^{13}C	10.7

Table1.3. Gyro magnetic Ratio of Common Nuclei [17].

Using Table 1.3 and Eq. (1.1), one can calculate the frequency needed for an RF coil for the most commonly imaged in MRI system.

Theoretically, Particles that have both odd atomic weight and atomic number like $H,^{1}C,^{13}F,^{19}P^{31}$ are non-zero spin which possesses the spin property and creates a small magnetic field or magnetic dipole moment around the proton. Such dipoles, when placed into a magnetic field, are expected to align with the direction of the magnetic field. These moving electrical charged particles create electric currents and, this is accompanied by the magnetic field.

From the theory of quantum mechanics, one can describe the relation between the spin angular momentum, $\hbar\vec{I}$ and the molecular magnetic moment, $\vec{\mu}$ by the following relation;

$$\vec{\mu} = \hbar\gamma\vec{I}, \tag{1.2}$$

where; $\hbar$ is Planck's constant divided by 2π, $\vec{I}$ is a dimension less angular momentum vector describing the intrinsic spin state, and γ is the which depends on the sign, size, and distribution of charge within the material. When placed in a magnetic field $\vec{B}$ these magnetic moments will polarize with energy:

$$E = -\vec{\mu}.\vec{B}. \tag{1.3}$$

If the magnetic field is oriented along the z -axis, $\vec{B} = B_0\hat{z}$, then $E = -\mu_Z B_0$. Hydrogen atoms, ^{1}H, consist of an electron orbiting a nucleus of a single proton. Since the proton has a spin quantum number $m = \left\{-\frac{1}{2},+\frac{1}{2}\right\}$ the hydrogen nucleus may exist in two spin states, either the 'up' state, $|\alpha\rangle$ or the 'down' state $|\beta\rangle$. When a dipole is subjected to a magnetic field, it will tend to align parallel or anti parallel with the direction of B_0 depending on whether its spin state is up or down. These parallel and anti-parallel states have a difference in energy, E_m, proportional to the strength of the magnetic field that the nuclei experience; this implies that the potential energy states are:

$$E_m = \left\{-\frac{\hbar\gamma B_0}{2}, +\frac{\hbar\gamma B_0}{2}\right\}. \tag{1.4}$$

This was experimentally verified by Rabi in 1938 [18].

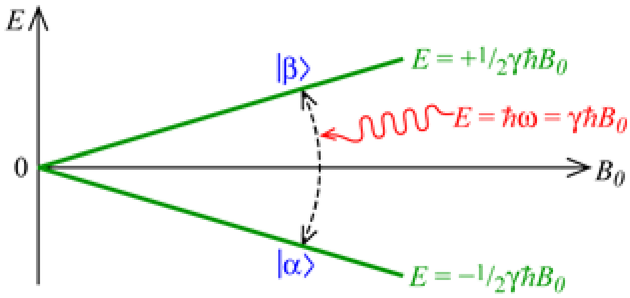

Figure 1.4: Energy level diagram of a spin, $\frac{1}{2}$ nucleus in a magnetic field, B_0.

If quantum of irradiated energy of magnitude $\gamma\hbar B_0$ is absorbed by the nuclei, the polarization of a particle will change to the higher energy state. By averaging over all possible spin states magnetization is given by;

$$M_0 = \rho\hbar\gamma \frac{\sum m e^{-E_m}/kT}{\sum e^{-E_m}/kT}, \tag{1.5}$$

where: ρ is the number of nuclei per unit volume and the summation is performed over all possible energy states. At room temperature, $E_m \leq KT$ and the exponential terms may be approximated by $(1-\frac{E_m}{kT})$. In general, for nuclei with spin I, this allows the magnetization to be approximated:

$$M_0 = \rho\hbar^2\gamma^2\left[\frac{I(I+1)}{3kT}\right]B_0, \tag{1.6}$$

continuing the example of one-half spin nuclei, i.e. $I = \frac{1}{2}$ and $m = \left\{-\frac{1}{2}, +\frac{1}{2}\right\}$, the magnetization vector is:

$$M_0 = \frac{\rho\hbar^2\gamma^2}{4kT}B_0. \tag{1.7}$$

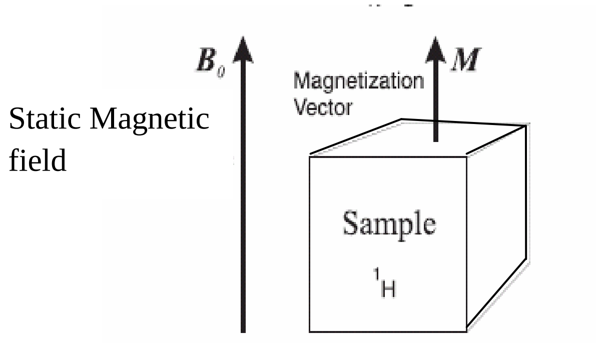

Figure1.5 Bulk Magnetization at Equilibrium

The significance of this relation is that the magnetization depends primarily on the quantum spin states I, the applied magnetic field B_0, the temperature T of the system, and the distribution ρ of the spins through the volume. The remaining parameters are intrinsic constants [19]. The MRI is that through manipulation of these magnetic moments; one can non-invasively construct an image.

1.3.2 Precession

When put in the external magnetic field, the individually aligned parallel or anti parallel protons spin in a particular way called precession. The speed of the precession is how many times the protons precess per second and is determined by the Larmor equation. The Larmor equation indicates that the frequency of the precession at higher field strengths is higher.

As shown in Section above, the motion of an ensemble of independent spin one-half nuclei in a magnetic field may be described in terms of the spin magnetization vector, M. By definition, the magnetization is proportional to the angular momentum L.

$$\vec{M} = \gamma \vec{L}, \tag{1.8}$$

where; the gyro magnetic ratio γ depends on the shape, size, and distribution of charge within the material. The torque acting on the magnetization in a magnetic field B is given as [20]:

$$\vec{\tau} = \frac{d\vec{L}}{dt} = \vec{M} \times \vec{B}, \tag{1.9}$$

combining these two equations, one obtains;

$$\frac{d\vec{M}}{dt} = \gamma \vec{M} \times \vec{B}. \tag{1.10}$$

When the magnetization is oriented parallel to $\vec{B}$, $\frac{d\vec{M}}{dt} = 0$. This is considered the equilibrium state. When $\vec{M}$ is not parallel to $\vec{B}$, the solution to Equation (1.10) when B is a magnetic field of amplitude $\vec{B}_0$ corresponds to a precession of the magnetization about the field at the rat $\vec{\omega}_0 = \gamma\vec{B}_0$ the Larmor frequency. For reference, the static magnetic field is assumed to be oriented along the positive *z* axis.

Therefore, precession is so common in MRI that it is useful to consider Eq. (1.10) in a reference frame rotating about the z-axis at an angular frequency ω. This "reference frame moment" is denoted $\vec{\omega}$. The velocity $\vec{v}$ of a particle in this rotating frame can be described by:

$$\vec{v} = v_\alpha \vec{\omega} \times \vec{r}, \tag{1.11}$$

where; v_α is the actual velocity in a fixed frame and the cross term represents the rotating frame translation to the fixed frame. If the magnetization is directed along r, the rate of magnetization change can be described by:

$$\frac{d\vec{M}}{dt} = \gamma \frac{dL}{dt} + \vec{\omega} \times \vec{M}. \tag{1.12}$$

Reducing Equation (1.12) to fit the form of Equation (1.9), we find

$$\frac{d\vec{M}}{dt} = \gamma\vec{M} \times (\vec{B}_0 - \frac{\vec{\omega}}{\gamma}). \tag{1.13}$$

Note that from the rotating frame perspective, as the frame precession approaches the Larmor frequency $\vec{\omega} = \gamma\vec{B}_0$. The phenomenon of resonance occurs with the application of a transverse B_1 field. This field must oscillate at a frequency $\vec{\omega}_0$ in order to tip the nuclei into a higher energy state. Such an oscillating field can be constructed from two circularly polarized fields rotating in opposite directions [21]:

$$2B_1 \cos(\omega_0 t) = B_1 e^{-i\omega_0 t} + B_1 e^{i\omega_0 t}. \tag{1.14}$$

If $B_{1<<} B_0$, then only the component rotating in the same sense as the magnetization needs to be considered. This allows the transverse magnetic field to be written as:

$$B_1(t) = B_1 \cos(\omega_0 t) - B_1 \sin(\omega_0 t). \tag{1.15}$$

Rewriting Equation (1.9) with both the longitudinal, B_0, and transverse, B_1, magnetic fields one finds:

$$\frac{dM_x}{dt} = \gamma\left[M_y B_0 + M_z B_1 \sin(\omega_0 t)\right], \tag{1.16}$$

$$\frac{dM_y}{dt} = \gamma\left[M_z B_1 \cos(\omega_0 t) - M_x B_0\right], \tag{1.17}$$

$$\frac{dM_z}{dt} = \gamma\left[-M_x B_1 \sin(\omega_0 t) - M_y B_1 \cos(\omega_0 t)\right], \tag{1.18}$$

with the solution

$$M_x = M_0 \sin(\omega_1 t)\sin(\omega_0 t), \tag{1.19}$$

$$M_y = M_0 \sin(\omega_0 t)\cos(\omega_1 t), \tag{1.20}$$

$$M_z = M_0 \sin(\omega_1 t), \tag{1.21}$$

Were $\omega_0 = \gamma B_0$, $\omega_1 = \gamma B_1$

This stationary frame solution shows that the magnetization tends to precess about both fields at the rates ω_0 and ω_1 respectively. The effect of the transverse field is more easily seen by shifting one's perspective to the frame rotating about the z-axis at ω_0. From this point, the magnetization appears to precess only about B_1 field. Thus, the effect of this transverse magnetic field is to rotate the net magnetization vector M away from the z-axis. This rotation occurs in the plane orthogonal to the applied B_1 field. The angle of rotation is controlled by the magnitude of the applied field and the length of time it is applied.

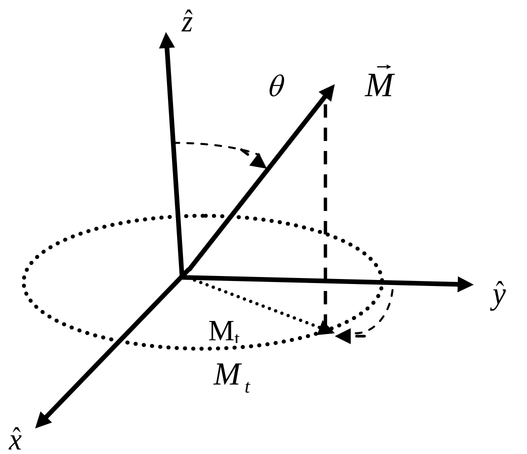

Figure: 1.6 Bulk Magnetization at Equilibrium Magnetization vector and transverse plane projection.

Typically, the physical coils that are used to apply the transverse B_1 field are the same coils used to acquire the imaging data. Thus, the magnitude of the received or recorded signal is proportional to the component of the magnetization that lies in the transverse plan. Applying a" 90^0, Pulse" rotates the magnetization vector completely into the transverse plane, and is typically the first step in the imaging process.

1.3.3 Excitation

The excitation process is the way to establish the phase coherence of individual magnetic moments, in order to generate a transverse magnetization. In fact, when the tissue is in the equilibrium state, there is not any transverse magnetization because all the phases are canceled with each other. For that reason that an external force must be applied at the spin system.

This force is the RF field B_1, generated at the RF coils, which is an oscillating field perpendicular to the main field. The rotation of this B_1 field is at the Lamor frequencies so that the energy exchange can be facilitate.

Any RF pulse that achieves a rotation of the net magnetization away from is thermal equilibrium orientation of parallel alignment is called excitation. In conventional MRI, this RF pulse is generated by means of a resonant cavity or near-field coil place either around or next to the tissue.

1.3.4 Reception

Following the application of an RF pulse, spins in the newly achieved high energy state will relax back to their low energy state. During relaxation, which occurs by two principle mechanisms, either by loss of energy to the environment spin-lattice or T_1 relaxation or loss of phase coherence spin-spin or T_2 relaxation, spins release the excess energy imparted by the RF pulse as a photon at the Larmor frequency. Different tissues, due to the different magnetic environments of their spins, relax at different rates by these two mechanisms, which can be used to generate image contrast.

1.3.5 Longitudinal and Transverse Magnetization

Opposing protons neutralize each other leaving a net number of protons parallel to B_O in the z-axis. The sum of magnetization is parallel to the external magnetic field and called longitudinal magnetization. Inside MRI, the patient acts as a bar magnet aligned with B_o which makes it impossible to measure the magnetic field of the patient as it is in the same direction as the external magnetic field.

The purpose of RF pulse is to distort the protons so they fall out of alignment with the external magnetic field. This only happens if the RF pulse has the same precessional frequency, which is called resonance. Thus, this magnetic resonance is set at the Larmor frequency. The RF field is also responsible for the spin tipping produced by the RF coil. The tip angle θ depends on the B_1 field, a time varying excitation perpendicular to the static magnetic field as well as its duration t as described in Eq. (1.22). The tipping of the magnetization can be seen from the rotating frame $\vec{M}$ itself as shown in Figure 1.7.

$$\theta = \gamma B_1 t. \tag{1.22}$$

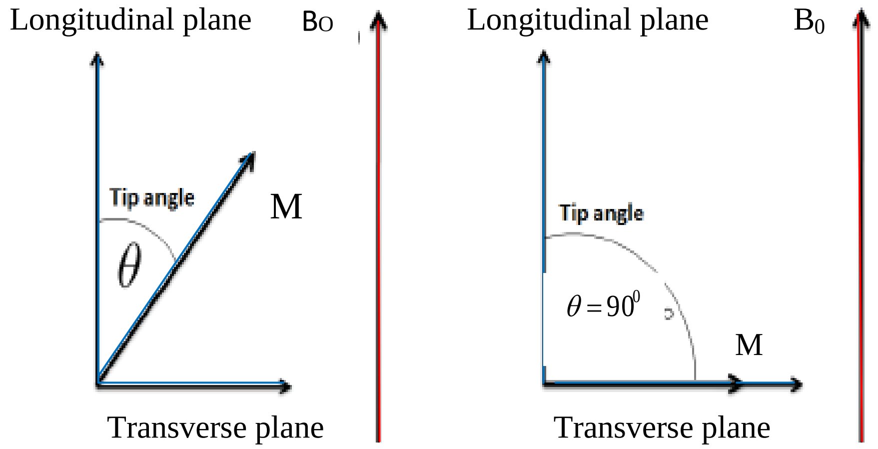

Figure 1.7: Flip angle of the magnetization *M* in the rotating frame of reference [22]

Two major effects happen during the activation of the RF pulse. First, some of the protons gain energy from the RF pulse and fall into the higher energy state, resulting in the reduction of longitudinal magnetization. Second, the RF pulse pushes the protons to synchronize in phase with each other instead of in random direction. This result is called transverse magnetization in which the net magnetization is the *x-y* plane with the precessing protons at the Larmor frequency.

Transverse magnetization is a moving magnetic field at Larmor frequency and if a receiver coil or antenna is placed near, an alternating voltage will be induced which generates electrical current. This current can be picked up to form MR signal. Immediately after the RF pulse is switched off, the protons start to fall out of phase and return to the lower energy state called relaxation. Relaxation occurs in two forms, T_1 and T_2 relaxation.

1.3.6 T_1 Relaxation

The T_1 relaxation process is also known as the longitudinal or spin-lattice relaxation time and describes the recovery of the M_Z component of the net magnetization vector as it returns to its equilibrium position along the z-axis after the application of the RF pulse. To relax back into equilibrium, the spins have to transfer the energy gained from the RF pulse to the environment. This transfer of energy is not spontaneous and can only happen if the spins experience an oscillating magnetic field at or near the Larmor frequency. The rate of energy transfer depends on a molecule's natural motions (rotation, vibration and translation). Hydrogen, in the form of water, is a small molecule and therefore, moves quite rapidly. Larger molecules, such as fat molecules move more slowly. The T_1 relaxation time reflects the relationship between the natural frequency of these molecules and the resonant or Larmor frequency. When these frequencies are similar, the T_1 recovery of Mo is rapid, when they are very different, the T_1 recovery is slow. In previous section the motion of magnetization vector was derived in Eq. (1.10) and (1.13) neglects the interaction between the protons and its surroundings.

In the case of any displacement of magnetization vector M from its original equilibrium position, it is this interaction that helps M to relax back to its initial position. The restoration of thermal equilibrium occurs primarily through a loss of energy between the spin system and the surrounding thermal reservoir often termed the lattice. This process is known as spin-lattice or longitudinal relaxation. The mathematical description of the process is given by:

$$\frac{dM_x}{dt} = -\frac{(M_z - M_0)}{T_1}, \tag{1.23}$$

with the solution:

$$M_z(t) = M_z(0)e^{-t/T_1} + M_0(1 - e^{-t/T_1}), \tag{1.24}$$

Following a 90^0 RF pulse, $M_z(0) = 0$ hence

$$M_z(t) = M_0(1 - e^{-t/T1}). \tag{1.25}$$

As seen in Figure 1.7, the spin-lattice is the relaxation time to reduce the difference between the longitudinal magnetization (M_z) and it's equilibrium by a factor of e [23].

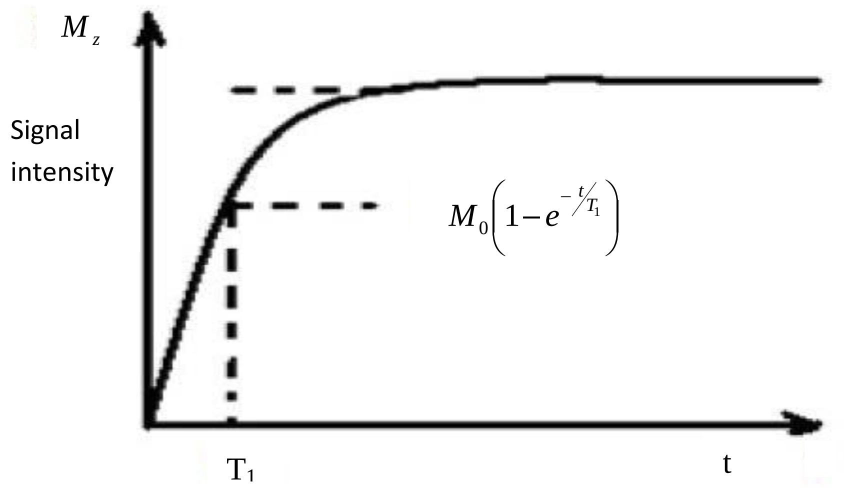

Figure 1.8: T_1 Relaxation

1.3.7 T_2 Relaxation

T_2 relaxation, also called spin-spin relaxation, describes how the protons fall out of phase in the *x-y* plane. There are two main causes for this loss of phase. The first, T_2 relaxation, results from a slowly fluctuating magnetic field with neighboring nuclei. This results in the random fluctuation of the Larmor frequency of individual protons causing an exchange of energy between proton spins, which leads to loss of phase coherence across a population of protons [24]. The second cause of phase is in homogeneity of static magnetic field B_0 causing slightly different Larmor frequencies for protons at different locations. T_2 is a constant describing the time taken for the M_{xy} to decay. The net magnetization in the *x-y* plane goes to zero, and the longitudinal magnetization grows until we have M_0 along *z*.

All of the longitudinal magnetization is rotated onto the x-y plane when a 90^0 pulse is applied and is represented as M_{xy} instead of M_z. This precesses about z axis inducing an alternating voltage of same frequency and analytically, the transverse relaxation process is given by:

$$\frac{dM_{xy}}{dt} = -\frac{M_{xy}}{T_2} \tag{1.26}$$

The solution after 90^o pulse is:

$$M_{xy} = M_{xy}(0)e^{-t/T_2} \tag{1.27}$$

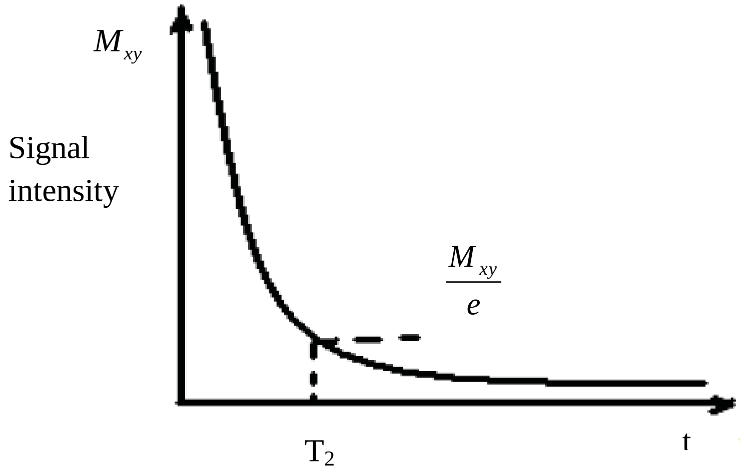

Figure 1.9: T_2 Relaxation

Since T_2 relaxation is solely the interaction between the spins, there is no transfer of energy to the surrounding tissues

The time-dependent behavior of M in the presence of an applied magnetic field B_1 (t) is described quantitatively by the Bloch equation. In the context of MRI, the Bloch equation takes the following general form of equation of motion for magnetization with relaxation parameter can be written as:

$$\frac{d\vec{M}}{dt} = \gamma\vec{M} \times \vec{B} - \frac{(M_z - M_0)\hat{z}}{T_1} - \frac{(M_x\hat{x} - M_y\hat{y})}{T_2}. \tag{1.28}$$

Under this mechanism, spins tend to align in the same direction as the external magnetic field.

Suppose that $B = B_0\hat{z}$ and the initial Magnetization of value $M = M_x, M_y, M_z$ if the relaxation times T_2 and T_1 is temporarily eliminated, the above equation becomes:

$$\frac{dM}{dt} = \gamma M \times B_0\hat{z}. \tag{1.29}$$

Each component of M can be written as:

$$\frac{dM_x}{dt} = \gamma B_0 M_y. \tag{1.30}$$

$$\frac{dM_y}{dt} = -\gamma B_0 M_x. \tag{1.31}$$

$$\frac{dM_z}{dt} = 0. \tag{1.32}$$

The precession can be easily obtained from the Eq. (1.30-1.32):

$$M_x(t) = M_x \cos\omega_0 t + M_y \sin\omega_0 t, \tag{1.33}$$

$$M_y(t) = M_y \cos\omega_0 t - M_x \sin\omega_0 t, \tag{1.34}$$

$$M_z(t) = M_0, \tag{1.35}$$

where ω_0 is defined as in Eq. (1.21). Taking the relaxation time T_2 and T_1 and into account, the solution becomes:

$$M_x(t) = (M_x \cos\omega_o t + M_y \sin\omega_o t)e^{-t/T_2}, \tag{1.36}$$

$$M_y(t) = (M_y \cos\omega_o t - M_x \sin\omega_o t)e^{-t/T_2}, \tag{1.37}$$

$$M_z(t) = M_z e^{-t/T_1} + M_o(1 - e^{-t/T_1}), \tag{1.38}$$

Generally, this solution indicates that the transverse component rotates with the Larmor frequency and exponentially decays to zero; the longitudinal component decays from the initial value M_x to its equilibrium value M_O.

After a magnetized spin system has been perturbed from its thermal equilibrium state by an RF pulse, according to the law of thermodynamics, return to this state, provide the external force is removed and sufficient time is given. This process is characterized by a precession of M about the B_O field, called free precession. Both relaxation processes are often described to the existence of time-dependent microscopic magnetic fields that surround a nucleus as a result of the random thermal motions present in an object.

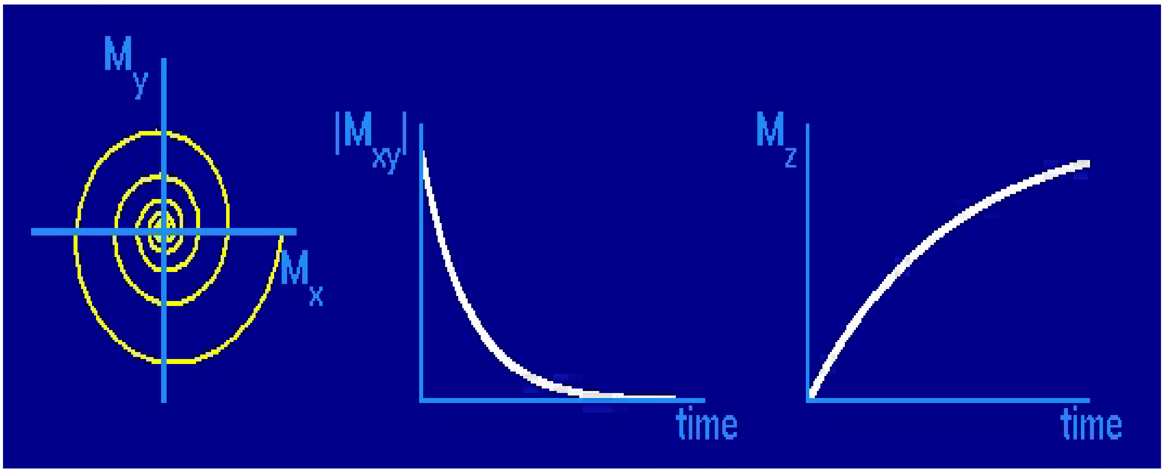

Precession Decay Recovery

Figure 1.10 Precessions and Relaxation (T_1 and T_2)

Contrast in MRI depends not only on the hydrogen density, but also on the additional properties of the sample described by the T_1 and T_2 relaxation time constants. These constants can be exploited to yield high quality images.

1.4 Radio frequency coil

The RF coils are used to produce the B_1 field necessary to rotate the spins and also detect the signal from the spins in the body tissue. They are used for transmitting and receiving signals in MRI. During transmission these coils produce a uniform magnetic field at the Larmor frequency, perpendicular to the $B_{0.}$ During reception, the coil detects the signal generated by the precessing sample as it relaxes back to its equilibrium state.

The basic principle behind the operation of an RF coil is Ampere's law, which states that a current passing through a wire generates a magnetic field.

$$\int \vec{J}.d\vec{s} = \frac{1}{\mu_0}\int \vec{B}.d\vec{l} \tag{1.39}$$

As shown in E.q. (1.39), $\vec{J}$ is representing the current distribution, B is magnetic field and μ_0 is permeability of free space.

Reception is based on the principle of Faraday Induction, which states that the rotating magnetic field produced by the sample induces an electromagnetic field (ξ) in the RF coil, in the opposite direction. This relation can be written as:

$$\zeta = \int \vec{E}.d\vec{l} = \frac{d}{dt}\int \vec{B}.d\vec{s} \tag{1.40}$$

Depending on their function, near-field RF coils are classified into three types: transmit only, receive-only coils and transmit-receive coils in which both the excitation of B_1 field and reception of MRI signal are achieved with the same RF structure.

In equilibrium, the net magnetization vector aligns with the main magnetic field along the z-axis. M_0 is several magnitudes smaller than B_0. In addition to this, M_0 is not an oscillating function, and hence cannot be detected by a receiver coil.

1.5 Signal detection

MRI signal detection is based on the well-known Faradays law of the electromagnetic induction. The faradays law of induction sates that the time-varying magnetic flux through a conducting loop (receive coil) will induce in the coil of an EM force or voltage that is equal to the rate at which the magnetic flux through the coil changing.

In MRI, the bulk magnetization is precession at a radio frequency and any conducting loop resonating at the frequency can be used as a receive coil. The induced emf in the loop coil is directly proportional to the time variation of magnetic flux through the coil.

$$emf = -\frac{d\Phi}{dt}, \tag{1.41}$$

where Φ is the magnetic flux going through the conductive coil area, which can be calculated by:

$$\Phi = \int_{coilarea} \vec{B}.d\bar{s} \tag{1.42}$$

The magnetic field generated by the bulk magnetization can be represented by an effective current density

$$\vec{J}_M(r,t) = \vec{\nabla} \times \vec{M}(r,t) \tag{1.43}$$

The vector potential at position r associated with this effective current density source is obtained from the Biot-Savart solution for the vector potential:

$$\vec{A}(r) = \frac{\mu_0}{4\pi} \int \frac{d^3 r' \vec{J}(r')}{|r - r'|}. \tag{1.44}$$

The integration is all over the whole bulk magnetization of image domain. The associated magnetic field strength can be found by:

$$\vec{B} = \vec{\nabla} \times \vec{A}, \tag{1.45}$$

substitute Eq. (1.45) into Eq. (1.42) and apply Stokes' theorem to obtain:

$$\Phi = \int_{looparea} \left(\vec{\nabla} \times \vec{A} \right) ds = \oint d\vec{l}.\vec{A}. \tag{1.46}$$

Therefore, the magnetic flux due to the bulk magnetization can be calculated by substituting Eq. (1.44) into Eq. (1.46) obtained as:

$$\Phi = \int d\vec{l}.\left[\frac{\mu_0}{4\pi} \int d^3 r' \frac{\vec{\nabla}' \times \vec{M}(r,t)}{|r - r'|} \right], \tag{1.47}$$

$$\Phi = \frac{\mu_0}{4\pi} \int d^3 r' \int d\vec{l}.\left[-(\vec{\nabla}' \frac{1}{|r - r'|}) \times \vec{M}(r,t) \right], \tag{1.48}$$

$$\Phi = \frac{\mu_0}{4\pi} \int d^3 r' \vec{M}(r,t).\left[\vec{\nabla}' \times (\int \frac{d\vec{l}}{|r - r'|}) \right], \tag{1.49}$$

$$\vec{B}^{recieve}(r') = \vec{\nabla} \times \left[\frac{\mu_0}{4\pi} \int \frac{d\vec{l}}{|r - r'|} \right]. \tag{1.50}$$

Assume that $\vec{B}_r^{receive}(r,t)$ is the laboratory frame magnetic field at location ***r*** produced by a hypothetical unit direct current flowing in the coil. Then, the magnetic flux though the coil by $\vec{M}(r,t)$

$$\Phi(t) = \int_{sample} \vec{B}^{receive}(r,t).\vec{M}(r,t)d^3r \qquad (1.51)$$

Then, according to the Faradays law of induction, the voltage V (t) induced in the coil is

$$Signal \propto -\frac{\partial \Phi}{\partial t} \propto -\frac{\partial}{\partial t}\int_{sample} \vec{B}^{receive}(,r,t).\vec{M}(r,t)d^3r \qquad (1.52)$$

The time varying magnetic fields associated with the precessing magnetization in MRI induce voltage in the MRI rf receive coil, giving to the MRI signal. The signal measured by some system of electronics is proportional to Eq. (1.52), which can be written out in terms of the individual components as:

$$s \propto -\frac{d}{dt} d^3r\left[\vec{B}_x^{receive}(r,t)\vec{M}_x(r,t) + \vec{B}_y^{receive}(r,t)\vec{M}_y(r,t) + \vec{B}_z^{receive}(r,t)\vec{M}_z(r,t)\right] \qquad (1.53)$$

The static-field solution Eq (1.36)-(1.38) holds for each r. The longitudinal generalization is

$$M_x(r,t) = M_z(r)e^{-t/T_1} + (1 - e^{-t/T_1}(r)). \qquad (1.54)$$

For static field at the Tesla (T) level and proton, the larmor frequency ω_0 the order of magnitude is larger than typical values of t/T_1 and r/T_2. Hence the derivative of the e^{-t/T_1} and e^{-t/T_2} factor most certainly can be eliminated or neglected; now the signal becomes:

$$signal \propto -\frac{d}{dt}\int\left[\vec{B}_x^{receive}(r,t)\vec{M}_x(r,t) + \vec{B}_y^{receive}(r,t)\vec{M}_y(r,t)\right]d^3r. \qquad (1.55)$$

The receive field in the laboratory components may be written as quite general in terms of the magnitude $B_\perp and d\theta_B$:

$$B_x^{receive} = B_\perp \cos\theta_B, \qquad (1.56)$$

$$B_y^{receive} = B_\perp \sin\theta_B, \qquad (1.57)$$

$$B_x^{receive}(r,t) + iB_y^{receive}(r,t) = B_\perp^{receive}(r,t)e^{i\theta_B}. \qquad (1.58)$$

And the Magnetization can be written as:

$$M_x(r,t) + iM_y(r,t) = M_\perp(r,o)e^{-(\omega_0 t - \phi_0(r))}e^{-t/T_2}. \qquad (1.59)$$

With the possible position dependence made explicit and the trigonometric identity:

$$\sin(a+b) = \sin a \cos b + \cos a \sin b, \tag{1.60}$$

$$s \propto \omega_0 \int d^3 r M_{\perp}(r,t) B_{\perp}(r) \sin(\omega_0 t + \theta_B(r) - \phi_0(r) e^{-t/T_2}. \tag{1.61}$$

Consider all quantities inside the integral Eq. (1.61) to be independent of r. If the sample volume is V_s, then:

$$s \propto V_s \omega_0 e^{-t/T_2} M_{\perp} B_{\perp} \sin(\omega_0 t + \theta_B - \phi_0). \tag{1.62}$$

To create the image, the MRI scanner uses radiofrequency field, gradient field, a static magnetic fields applied to the body or body part of interest, in such a way that a measureable signal will be emitted from the tissue.

Therefore, the MRI signal is proportional to the coil sensitivity, transverse magnetization, volume of sample. For the precession frequency to be constant everywhere, the static field B_0 must be uniform throughout space.

For the increasing of B_1 field there will be also high signal mean while B_1 field approximately zero there will be no MRI signal.

Generally, the MRI signal is directly proportional to the B_1 field.

$$Signal \propto B_{\perp}\, field. \tag{1.63}$$

1.6 Thesis Structure

This thesis is composed of four chapters. Begins with a brief introduction to the physics of MRI, background of EM vacuum and motivation of thesis are outlined in Chapter 1 and Principles of MRI is presented. A comprehensive literature review, including EM field in free space, Skin depth, and EM vacuum in conductors, EM field analysis and basic RF field concepts with their performance evaluation processes is provided in Chapter 2.

In Chapter three, B_2 field calculation inside cylindrical shell of finite thickness and infinite length due to excitation by concentric finite coil placed inside the shell. The calculation is made analytically using separation of variables methods and the result is present interims of modified Bessel function. The skin depth effect is seen as result of simulation is addressed and also the results and discussions are shown. Chapter four summary and concludes of findings within this thesis.

Chapter Two

2 Literature Review

2.1 EM wave in Conductors

Electromagnetic waves in free space are characterized by amplitude that remains constant in space and time. This is also true for waves travelling through any isotropic, homogeneous, linear, non-conducting medium, which we may refer to as an ideal dielectric.

To understand the shielding effect of good conductors is relatively straightforward. Essentially, we follow the same procedure to derive the wave equations for the EM fields as we did for the case of a vacuum, but we include additional terms to represent the conductivity of the medium. These additional terms have the consequence that the amplitude of the wave decays as the wave propagates through the medium. The rate decay of the wave is characterized by the skin depth, which depends on the conductivity of the medium and frequency of the EM wave. Inside a conductor, free charges can move or migrate around in response to EM fields contained therein, as we saw for the case of the longitudinal magnetic field inside a current-carrying wire that had a static potential difference across its ends. Even in the static case of electric charge residing on the surface of a conductor, we saw that $\vec{E}_{inside}(\vec{r})=0$, but actually mean that the net electric field inside the conductor is zero. From Ohm's Law, we know that the free current density $J_{free}(r,t)$ is proportional to the electric field inside the conductor.

$$\vec{J}_{free}(r,t)=\sigma_c\vec{E}_{inside}(r,t)=\frac{\vec{E}_{inside}}{\rho_c}(r), \tag{2.1}$$

where: σ_c Conductivity of the metal conductor and ρ_c charge density with this the, Maxwell equation for linear media assume the form [25].

$$\vec{\nabla}.\vec{E}(r,t)=\frac{\rho_c}{\varepsilon}(r,t) \tag{2.2}$$

$$\vec{\nabla}.\vec{B}(r,t)=0 \tag{2.3}$$

$$\vec{\nabla}\times\vec{E}(r,t)=-\frac{\partial\vec{B}}{\partial t}(r,t) \tag{2.4}$$

$$\vec{\nabla}\times\vec{B}(r,t)=\mu\varepsilon\frac{\partial\vec{E}}{\partial t}(r,t)+\mu\sigma\vec{E}(r,t). \tag{2.5}$$

Electrical charge is always conserved, thus the continuity equation inside the conductor holds and is given by:

$$\vec{\nabla}.\vec{J}_{free}(r,t) = -\frac{\partial \rho_{free}}{\partial t}(r.t), \tag{2.6}$$

$$\text{But} \quad \vec{J}_{free}(r,t) = \sigma_c \vec{E}_{inside}(r,t), \tag{2.7}$$

$$\sigma_c(\vec{\nabla}.\vec{E}(r,t)) = \frac{\partial \rho_{free}}{\partial t}(r,t), \tag{2.8}$$

$$\nabla.\vec{E}(r,t) = \frac{\rho_{free}}{\varepsilon}(r,t), \tag{2.9}$$

$$\sigma_c \frac{\rho_{free}}{\varepsilon}(r,t) = -\frac{\partial \rho_{free}}{\partial t}(r,t), \tag{2.10}$$

$$\frac{\partial \rho_{free}}{\partial t}(r,t) + \left(\frac{\sigma_c}{\varepsilon}\right)\rho_{free}(r,t) = 0. \tag{2.11}$$

The general solution of this differentail equation for the free charge density is the form;

$$\rho_{free}(r,t=o) = \rho_{free}(r,t=0)e^{-(\sigma/\varepsilon)t} \tag{2.12}$$

$$\rho_{free}(t) = \rho_{free}(0)e^{\frac{-t}{\tau_{rlax}}} \tag{2.13}$$

So the free charge density decays on a timescale which is the relaxation time. If this is small, then any free excess charge is quickly rearranged away and the medium is a good conductor. A perfect conductor would have this timescale tending to zero. Thus, the continuity equation $\vec{\nabla}.\vec{J}_{free}(r,t) = -\frac{\partial \rho_{free}}{\partial t}(r,t)$ accumulated inside a good conductor tells us that any free charge density $\rho_{free}(r,t) = 0$ initially present at time is exponentially damped.

The free charge density dissipates in a characteristic time $\tau = \frac{\varepsilon}{\sigma_c}$. Similar to the static case in which the charge will flow to the edge of the conductor.

For a poor conductor $\sigma_c \to 0$ then $\tau_{relax} = \frac{\varepsilon}{\sigma_c} \to \infty$

2.2 Skin Depth Effect

Skin depth effect is the tendency of an alternating electric current to become distributed with in conductor such that the current density is largest near the surface of the conductor and decrease with greater depth in the conductor.

Knowledge of the electrical current distributions in conductors is important in many fields of research involving the development of electrical devices (e.g. transformers, inductors, electric motors), high current applications, superconductive materials), batteries, fuel cells, to name a few be consistent in RF (J .Magn. Reson. Imaging (1995) [26]. In general the current distribution in a conductor depends strongly on the current frequency, the shape and size of the current function, and the shape and material of the conductor itself A.J. Ilotta (2014) [27]. Electrical alternating currents in massive conductors have a tendency to be displaced from the core to the surface (skin) due to the interaction between eddy currents in different regions of the material. This phenomenon is known as the skin effect. The skin depth effect is defined as the required thickness of a metal of EM field of RF signal to be reduced 37 $\%$ of its original strength [28]. The eddy current skin-effect limits the detection of subsurface defects and the range of thickness measurement.

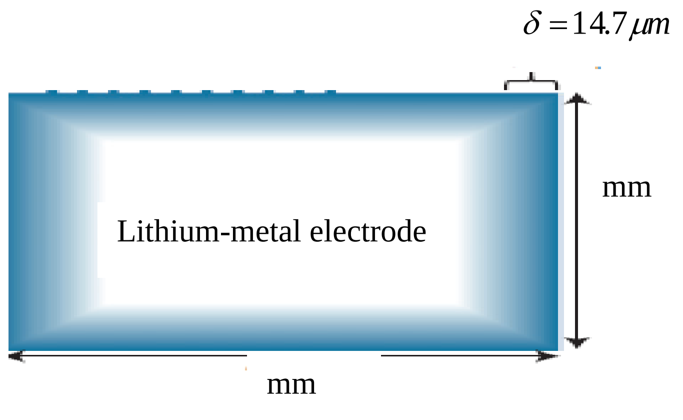

Figure, 2.1: Schematic showing the radiofrequency penetration in a block of lithium metal and immersed in 3D plane wave [29] (Where $\mu = 17.6\times10^{-2} m kg A^{2} S^{-2}$ $\rho = 92.8 n\Omega m$ $\omega = 219.8 MHz$ and the magnetic field strength is 21T.

The fraction of the metal block excited by the radiofrequency field depends on the δ and its surface area. The intensity of the blue colure depicts the strength of the B_1. The white region Furthermore, edges and corners typically produced large signal in any orientation.

The MRI approach describes here relies on the finite ability of the B_1 used to excite the Li nuclei, to penetrate the bulk Li metal electrode beyond tens of micrometer, said to skin depth problem. The skin depth depends on the type of metal (i.e., its resistivity and permeability) and also the Larmor frequency.

The δ can be easily calculated because it is a function of known physical constants and the properties of the relevant metal: The skin depth can be calculated by:

$$\delta = \sqrt{\frac{2\rho}{\pi\mu\omega_{rf}}}, \qquad (2.23)$$

where σ is the conductivity of the conductor (metal), μ its Magnetic permeability, skin depth is considered, however, it turns out that thickness is only critical at low with $\omega_{r.f}$ is the frequency of the applied r.f field:

$$\mu = \mu_0\mu_r, \quad \sigma = \frac{1}{\rho} \qquad \omega_{r.f} = 2\pi\nu,$$

where: μ is magnetic permeability

μ_0 the free space permittivity $\mu_0 = 4\pi \times 10^{-2} m\,kgA^{2}s^{-2}$

ρ is the resistivity of the metal (92.8n Ω m) for Li

μ_r is the relative Permeability of the metal Li 1.4

And $v_{r.f} = 350MHz$,is the frequency of the applied r.f field ,set to the resonance frequency for Li in a magnetic field of strength 21T. When using in Eq. (2.23), these values yields $\delta \approx 14.7\mu m$ is calculated for Li. Note that the use of a higher magnetic field strength for MRI will be lead to a smaller skin depth. As radiofrequency only penetrates the subsurface region, the bulk metal signal is proportional to the area of the metal, not to its volume in the above figure (2.1).

However, at low frequencies, permeability would increase the skin depth and improve magnetic field characteristics and it reduces the effective cross section of the conductor.

The RF EM fields, upon encountering bulk metal, face the phenomenon of skin effect. Of particular interest to this journal is the fact that the magnitude of the B_1 field decays exponentially inside the metal [30-31]. The RF field strength B_1 inside a metal decreases as a function of the depth y from the surface as given by: [32].

$$B_1(y) = B_1(0)e^{(-\frac{y}{\delta})}. \quad (2.25)$$

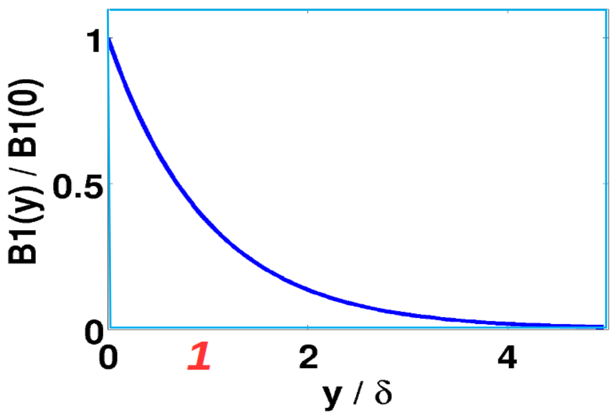

Figure .2.2. Exponential decay of magnitude of $B_1(y)$, as the function of the depth from the metal surface.

For the large number of the skin depth the RF will be limited mean while the attenuated signal is formed. This leads to decreasing MRI signal.

As the radiofrequency only penetrate the subsurface region, the bulk metal signal is proportional to the area of the metal. The flip angle is defined as the angle to which the net magnetization is rotated or tipped relative to the main magnetic field direction by the application of a RF excitation pulse at the Larmor frequency. Ernst and Anderson [33] long ago presented an expression for estimating the achieved flip angle in the case of small off-resonance excitation. The flip angles when the off-resonance excitation frequency is comparable to γB_1 (where B_1 is a magnitude of the RF field) [34].

$$\text{Flip angle: } \theta = \int_0^{\tau} \omega_1(t)dr \quad \text{but } \omega_1 = \gamma B_1 \ , \quad (2.26)$$

$$\theta_0 = \theta(0) = \gamma B_1(0)\tau, \quad (2.27)$$

where: θ is the r.f flip angle of the metal surface γ is the gyro magnetic ratio for Li, τ is the duration of the applied r.f. pulse.

Consider a face parallel to B_1 using Eq. (2.25) the subsurface side of the face, per unit area, contributes to the signal according to [32].

$$signal \propto \int_0^\infty \sin(\theta_0 e^{-\frac{y}{\delta}})dy, \tag{2.28}$$

$$signal \propto \delta \int_0^{\theta_0} \sin(\theta_0 e^{-\frac{y}{\delta}}) \propto \delta_{eff}, \tag{2.29}$$

where, δ_{eff} is the effective subsurface depth contributing to the signal, in the absence of exponential decay of B_1 in Fig (2.3) below. We can generalize the proportionality above to an arbitrary elemental surface area perpendicular to y and the exponential decay with y causes attenuation of the EM field.

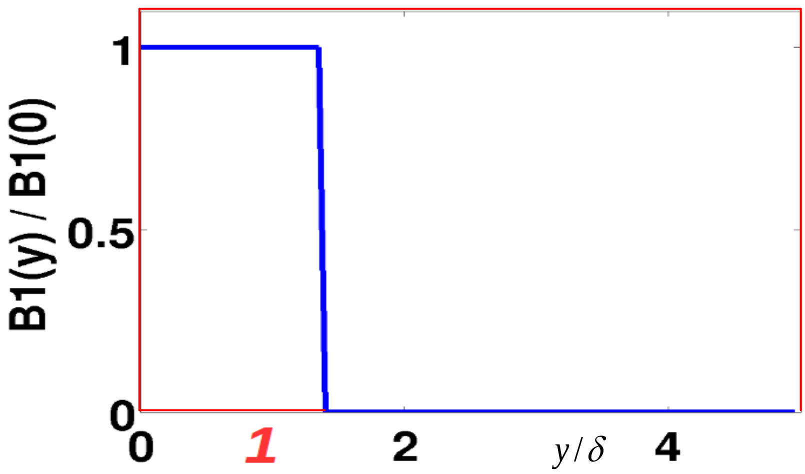

Figure.2.3. Effective subsurface depth δ_{eff}, without B_1 decay, that would account for the MRI signal [32].

The amplitude of an EM field propagates through conductor decay exponentially of a characteristic length scale. Consequently, an EM field cannot penetrate more than a few skin depths in to a conducting medium. It can be seen that the skin depth for a good conductor decrease with increasing wave frequency.

2.3 Electromagnetic field analysis

A linearly polarized RF field travelling in a given direction may be expressed as [35].

$$\vec{\nabla}^2 H_y - k^2 H_y = 0, \tag{2.30}$$

where , H_y is the single component of the magnetic field and k is a propagation constant.

Our magnetic field problem is effectively a plane wave travelling in a source free lossy media hence the square of the propagation constant is [36].

$$k^2 = j\omega\mu(\sigma + j\omega\varepsilon). \tag{2.31}$$

The propagation constant k is the sum of attenuation and phase constants, which are typically denoted as α and β, respectively (i.e. $k = \alpha + j\beta$) .Rewriting Eq.(2.31) in terms of α and β

$$\alpha = \omega\sqrt{\mu\varepsilon}\left\{\frac{1}{2}\left[\sqrt{1+\left(\frac{\sigma}{\omega\varepsilon}\right)^2} - 1\right]\right\}^{\frac{1}{2}}, \tag{2.32}$$

$$\beta = \omega\sqrt{\mu\varepsilon}\left\{\frac{1}{2}\left[\sqrt{1+\left(\frac{\sigma}{\omega\varepsilon}\right)^2} + 1\right]\right\}^{\frac{1}{2}}. \tag{2.33}$$

The attenuation constant α is expressed and shows the attenuation of the field as it propagates through a medium. The phase constant β in will determine the amount of phase shift. The distance the wave must travel in a lossy medium to reduce its value by a factor of e^{-1} is defined as the skin depth. The skin depth is defined as the required thickness of the metal from an RF signal to be reduced 37% of its original strength [29].

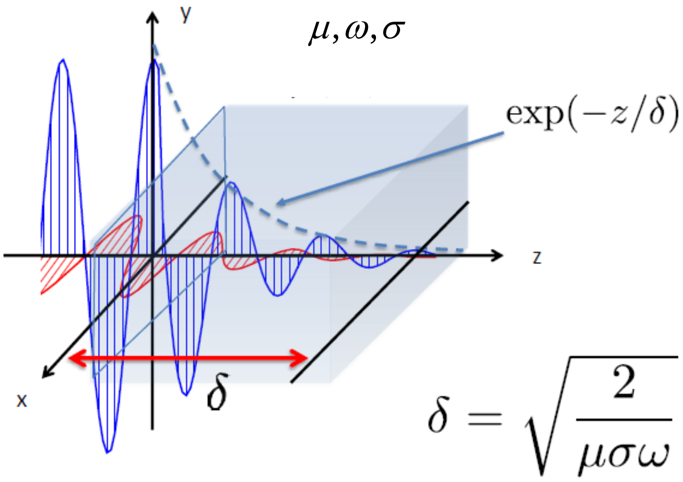

Fig. 2.4 skin depth

$$\delta = \frac{1}{\alpha}. \tag{2.34}$$

The skin depth gives a measure of the average depth of penetration of the RF fields. B_1 fields are critical to nuclear excitation and signal reception in MRI. The integration between these fields and human tissue in anatomical geometry results in variety of effects regarding image integrity and safety of human body. The two most important health related properties of EM fields are frequency and field strength. Low-frequency fields can cause the generation of electric current in the body. While high frequency fields can be lead to heating up of the body or parts of the body.

Here, has reviewed the basic physics of radiofrequency EM vacuum inside a bulk metal strip by MRI. The combination of increasing complexity of B_1 field techniques and technology in MRI makes this much more challenging today.

Here, the fundamental roles of the calculation of B_1 fields in EM vacuum are discussed after excitation inside shell and the shell of finite thickness, consisting of cylindrical shell and we observe that the skin depth is inversely proportional to $\sqrt{\omega\sigma}$, which indicate that field's penetration is more difficult at higher frequency and in better conductor.

In fact, they encounter strong resistance when they try to penetrate in conductors and in region outside the material the conductivity is zero ($\sigma = 0$) and the conducting material is non-magnetic.

The aim of this thesis work is to calculate B_1 field inside cylindrical shell of finite thickness and infinite length due to excitation by concentric finite coils placed inside the shell due to circular loop and visualizing EM vacuum inside in a metal object. For large value r and maximum skin depth of EM field will be attenuate and mean while the magnetic field will decrease and no signal is detected. And this region is EM vacuum. The RF field is strength varies as function of the distance from the surface. Therefore, the MRI signal is directly proportional to B_1 fields.

Chapter Three

3.1 General Description of the problem

A cylindrical shell of finite thickness and infinite length is considered, with the current assumed to flow in a coil placed inside the shell at a distance b from its axis fig3.2. The problem is to find magnetic field inside cylindrical shell of finite thickness and infinite length due to excitation due to circular loop. The magnetic field is perpendicular to the axis of the cylinder and decays with as a result of skin depth effect. For small value of radial distance there will be high signal due to by B_1 field and image is formed. For large value of skin depth of EM field will be attenuate and mean while the magnetic field will be decrease and no signal will detects at that region. Therefore, MRI is the only method to visualizing EM vacuum.

3.2 Quasi-Static Approximation and Skin Depth

EM field calculation using a quasi-stationary approximation in this section is in which the displacement current is much smaller than the conduction current and can be ignored. To make this statement clear, formulas describing magnetic field can be written down from Maxwell equations as follows.

$$\vec{\nabla} \times \vec{E} = -\frac{\partial \vec{B}}{\partial t}, \tag{3.1}$$

$$\vec{\nabla} \times \vec{B} = \mu \vec{J}_C + \mu \vec{J}_D, \tag{3.2}$$

where μ is the magnetic permeability, $\vec{J}_C$ is the conduction current density and $\vec{J}_D$ stands for the displacement current density which has the following expression:

$$\vec{J}_D = \varepsilon \frac{\partial \vec{E}}{\partial t}, \tag{3.3}$$

According to Ohm's law we also know that:

$$\vec{J}_C = \sigma \vec{E} \tag{3.4}$$

ε, σ are the electric permittivity and conductivity respectively. Substituting Eq. (3.3) and (3.4) back into Eq. (3.2) we get:

$$\vec{\nabla} \times \vec{B} = \mu \left(\sigma + \varepsilon \frac{\partial}{\partial t} \right) \vec{E} \tag{3.5}$$

For current with low frequency and flowing in high conductive media $\frac{\sigma}{\varepsilon\omega} >> 1$, the second term on the right of Eq. (3.5) can be dropped (this is true for low field MRI), which the quasi-stationary approximation is made in magnetic field calculation. So Eq. (3.5) becomes:

$$\vec{\nabla} \times \vec{B} = \mu\sigma\vec{E}. \tag{3.6}$$

Taking the curl on both sides of Eq.(3.6) and using the vector algebra $\vec{\nabla} \times \vec{\nabla} \times \vec{B} = \vec{\nabla}.\vec{B} - \vec{\nabla}^2\vec{B},$ then equation (3.6) became and by using the fact that $\vec{\nabla}.\vec{B} = 0$ and Eq. (3.1), Eq. (3.6) can be rewritten as:

$$\vec{\nabla}^2.\vec{B} = \mu\sigma\frac{\partial\vec{B}}{\partial t}. \tag{3.7}$$

Actually, current density and the magnetic vector potential satisfy equations of the same form as Eq. (3.7). There is a skin depth concept associated with magnetic to explain it, let us consider or suppose a finite conductor occupies the space $z \geq 0$ as shown in Figure 3.1 below. The surface $z = 0^-$ is subjected to a harmonic oscillating magnetic field, which is spatially uniform and pointing to the x-direction [37].

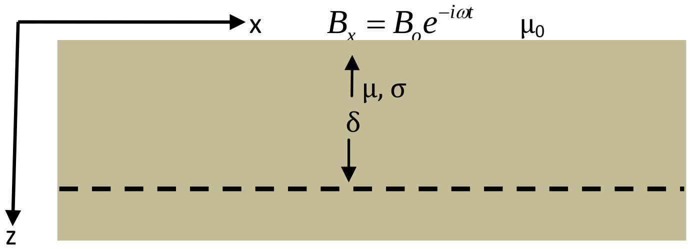

Figure 3.1 a spatial uniform magnetic field is applied to the surface $z = 0^-$ of a conductive medium.
Localized magnetic field and exist in the region at the order of several skin depths [37].
The solution for magnetic field in the semi-infinite conductive material can be easily obtained by solving Eq. (3.7) in Cartesian coordinate and applying appropriate boundary conditions [38].

$$\vec{B}(z,t) = \vec{B}_0 e^{(z/\delta - \omega t)} e^{-z/\delta}, \tag{3.8}$$

where, δ is a quantity describing how far the field can penetrate through the media which is called skin depth:

$$\delta = \sqrt{\frac{2}{\mu\omega\sigma}}. \tag{3.9}$$

The skin depth is a measure of how deep the magnetic field can penetrate in to the conductor. We observe that the skin depth is inversely proportional to frequency and conductivity, which indicates that field penetration, is more difficult at higher frequency, and in better conductor. Therefor, the skin depth could be very small for material with high conductivity. In MRI applications, passive shields (e.g. the gradient shield or the RF shields) made by high conductive materials are utilized to screen the fringe field.

Since MRI signal is proportion to field penetration, we can see that the signal will decay $e^{-z/\delta}$ inside the material.

3.3 Magnetic Field semi- infinite planar model

The magnetic induction B, in a linear, homogenous and isotropic medium must satisfy the wave equation [39].

$$\vec{\nabla}^2\vec{B} - \varepsilon\mu\frac{\partial^2\vec{B}}{\partial t^2} - \mu\sigma\frac{\partial\vec{B}}{\partial t} = 0 \tag{3.10}$$

where ε is the permittivity, μ is permeability and σ the conductivity of the medium.

The above expression or Eq. (3.10) which describes the behavior of a sinusoidal time dependent magnetic induction field in a semi-infinite plane of conducting material is the same as that which describes of plane electromagnetic wave in conducting media. Thus, the conducting material which occupies the $x \geq 0$ region is subjected to the magnetic induction field [40].

$$\vec{B}(x \geq 0) = \vec{B}_0 e^{j\omega t}\hat{z} \tag{3.11}$$

Then with in medium

$$\vec{B}(x \geq 0) = \vec{B}_0 e^{-K_I x + j(\omega t - K_R x)\hat{z}} \tag{3.12}$$

$$K_I = \omega\left(\frac{1}{2}\varepsilon\mu\{[1 + (1/\rho^2\varepsilon^2\omega^2)]^{\frac{1}{2}} - 1\}\right)^{\frac{1}{2}} \tag{3.13}$$

$$K_R = \omega\left(\frac{1}{2}\varepsilon\mu\{[1 + (1/\rho^2\varepsilon^2\omega^2)]^{\frac{1}{2}} + 1\}\right)^{\frac{1}{2}} \tag{3.14}$$

And ω is the angular frequency, and where it is understood that we are considering only the real parts of eq. (3.11) and (3.12).

The reciprocal of the imaginary part K_I of the wave number, is the distance over which the amplitude of the field is attenuated by a factor 1/e and is the skin depth of the medium [41] The real part, $K_R(= 2\pi/\lambda)$, where λ is the wavelength in the medium), gives rise to a change phase with position in the material.

3.4 Cylindrical model

Here we can consider an infinitely long cylinder of radius r_0, of the conducting material coaxial with the z -axis and immersed in the alternating magnetic field described by above eq. (3.11). By symmetry the field inside the cylinder will be a function of the radial position coordinate only, and if we assume a solution of (3.10) of the form [42].

$$\vec{B} = \vec{B}_0 R(r) \exp^{j\omega t} \hat{z}. \tag{3.15}$$

Therefore the function R(r) must satisfy the modified Bessel equation:

$$\frac{\partial^2 R}{\partial r^2} + \frac{1}{r}\frac{\partial R}{\partial r} - K^2 R = 0, \tag{3.16}$$

of order zero and independent variable Kr, where $K = K_I + jK_R$ is the complex wave number. The solution of **(**3.16**)** that remains finite for all $r \le r_0$ is:

$$R(r) = \frac{I_0(Kr)}{I_0(Kr_0)}, \tag{3.17}$$

where I_0, is a modified Bessel function of the first kind of order zero, and the integration constant, $[I_0(Kr_0)]^{-1}$ has been chosen so that R(r) = 1 at $r = r_0$. This result is similar to that which describes uniform cylindrical electromagnetic waves with the B vectors parallel to the axis. Eq. (3.17) can be expressed in polar form by expanding the modified Bessel function into a power series (Spiegel 1968**)** and invoking De Moivre's formula [43]. Thus the solution (3.15) can be written as:

$$\vec{B} = \vec{B}_0 \frac{|I_0(Kr)|}{|I_0(Kr_0)|} e^{j(\omega t - \xi(r))} \hat{z}, \tag{3.18}$$

$$\text{where} \quad |I_0(kr)| = \left[\operatorname{Re} I_0(kr)^2 + I_m I_0(kr)^2\right]^{\frac{1}{2}}. \tag{3.19}$$

Here the attenuation in amplitude of the magnetic field is described by the ratio $|I_0(kr)|/|I_0(kr_0)|$ and the phase variation is described by $\xi(r)$. The infinite series $\operatorname{Re} I_0(kr)$ and $\operatorname{Im} I_0(kr)$ converge rapidly in practice.

3.5. Field due to circular loop excitation inside a Cylindrical Shell

3.5.1. Excitation inside shell and shell of finite thickness

The distribution of the field due to excitation are calculated in a geometrical configuration consisting of a cylindrical shell of the infinite length and finite thickness, excited by a finite number of concentric current loops placed coaxially at a known position along the axis of the tube. The function giving the distribution of the field due to excitation is expressed in integral form. Figure .3.2. Indicate that a cylindrical shell metal excited in circular loop.

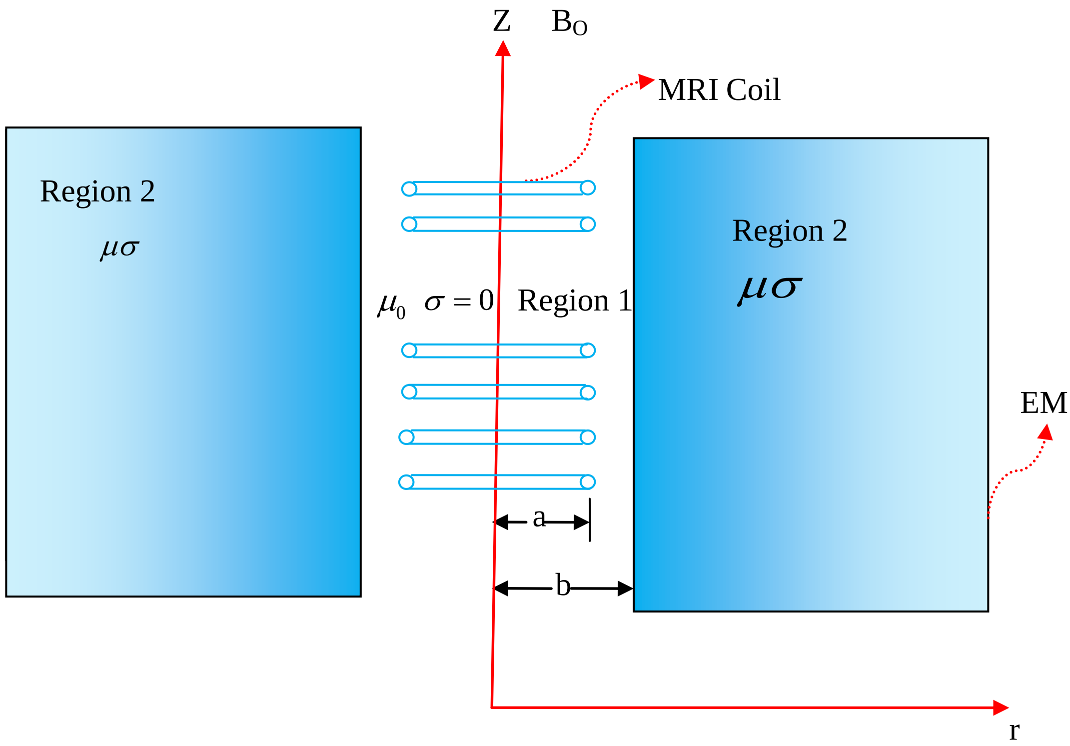

Fig 3.2 Schematic diagram of cylindrical shell exited by concentric current loops.

The circular loops may be considered connected in series to form a coil with a current with harmonic time variation flowing in this coil. The material of region **2** has conductivity σ and a constant magnetic permeability μ .For the solution it is the assumed that the displacement current can be neglected, because power frequency is used and the dimensions of the apparatus are small compared with the corresponding wavelength. It is also assumed that the circular loops of radius *a* are placed along the axis of a hole of radius *b* in region **1,** which is non-conducting and non-magnetic.

The field of the induced field due to excitation within the material of region **2** at any point varies both the radial distance ***r*** and the axial distance ***z.*** There is no variation with the

r

coordinate φ since the loops are placed at the center of the hole and the excitation current does not vary with the coordinates φ .

Magnetic vector potential satisfies the differential equations are used. The general equations used are as follows [44]:

$$\vec{\nabla}^2 \vec{A}_1 = 0 \text{ Outside the shell material (region}\mathbf{1}\text{)}, \tag{3.19}$$

$$\vec{\nabla}^2 \vec{A}_2 = \mu\sigma \frac{\partial \overline{A}_2}{\partial t} \text{ Inside the shell material (region}\mathbf{2}\text{)}, \tag{3.20}$$

where, $\mu = \mu_r \mu_0$ the magnetic permeability of the conductor material and σ its conductivity. Cylindrical co-ordinates are used. Using a system of cylindrical coordinates (r, φ, z) with unit vector $\hat{r}_0, \hat{\varphi}_0, \hat{z}_0$ and the fact that the components $A_{1,z}, A_{2,z}, A_{1,r} A_{2,r}$ are equal to zero and also that the components $A_{1,\varphi}$ and $A_{2,\varphi}$ are independent of the coordinate of φ and that the time variation is harmonic, the vector $\vec{A}_1$ and $\vec{A}_2$ are given by the following expressions [45].

$$\vec{A}_1(r,z,t) = \vec{A}_{1,\varphi}(r,z)e^{j\omega t}\hat{\varphi}_0, \tag{3.21}$$

$$\vec{A}_2(r,z,t) = \vec{A}_{2,\varphi}(r,z)e^{j\omega t}\hat{\varphi}_0 \tag{3.22}$$

Substituting from Eq. (3.21) and Eq. (3.22) in to Eq. (3.19) and Eq. (3.20), we obtain the following differential equations for the components $A_{1,\varphi}(r,z)$ and $A_{2,\varphi}(r,z)$:

$$\frac{\partial^2 \vec{A}_{1,\varphi}}{\partial r^2} + \frac{1}{r}\frac{\partial \vec{A}_{1,\varphi}}{\partial r} - \frac{\vec{A}_{1,\varphi}}{r^2} + \frac{\partial^2 \vec{A}_{1,\varphi}}{\partial z^2} = 0, \tag{3.23}$$

$$\frac{\partial^2 \vec{A}_{2,\varphi}}{\partial r^2} + \frac{1}{r}\frac{\partial \vec{A}_{2,\varphi}}{\partial r} - \frac{\vec{A}_{2,\varphi}}{r^2} + \frac{\partial^2 \vec{A}_{2,\varphi}}{\partial z^2} = jp^2 \vec{A}_{2,\varphi}, \tag{3.24}$$

where $p^2 = \omega\mu\sigma.$

For the general solution of Eq. (3.23) and Eq. (3.24) the method of separation of variables for the function $A_{1,\varphi}$ and $A_{2,\varphi}$ is applied. The magnetic vector potential in region **1** is the sum of $\vec{A}'_1$ due to the excitation and $\vec{A}_1''$ due to the induced magnetic fields within the conducting material of region **2**

$$\overline{A}_1(r,z) = \overline{A}_1'(r,z) + \overline{A}_1''(r,z) \tag{3.25}$$

The magnetic vector potential $\vec{A}_1' = \sum_{i=0}^{N} \vec{A}_{1,i}'$ .Eq. (3.32) for the component $\vec{A}_{1,\varphi}$ is written

$$\vec{A}_{1,\varphi}(r,z)=\sum_{i=0}^{N}\vec{A}'_{1,i,\varphi}(r,z)+\sum_{i=0}^{N}\vec{A}''_{1,i,\varphi}(r,z). \quad (3.26)$$

The magnetic vector potential of a circular loop of the radius **a** in an unbounded space is given by the expression [46]

$$A_{\varphi}'(r,z)=\frac{\mu I}{2\pi}\int_{0}^{\pi}\frac{a\cos\varphi d\varphi}{\left(a^2+r^2+z^2-2ar\cos\varphi\right)^{1/2}}. \quad (3.27)$$

This can be transformed in to the form [45]

$$A'_{\varphi}(r,z)=\frac{\mu aI}{\pi}\int_{0}^{\infty}K_1(kr)I_1(ka)\cos kz dk, \quad (3.28)$$

and for the i[th] loop [47]

$$A'_{i,\varphi}(r,z)=\frac{\mu aI}{\pi}\int_{0}^{\infty}K_1(kr)I_1(ka)\cos k(z-ih)dk, \quad (3.29)$$

where I_1 and K_1 are modified Bessel function.

In the expression only the Bessel function K1 is used, because the vector potential due to excitation inside the material vanishes as we move away to ward infinity.

Applying the method of separation of variables to Eq. (3.24) and considering that $A_2(r,z)=R_2(r).Z_2(z)$, we may write two differential equations as follows:

$$\frac{d^2R_{2,i}}{dr^2}+\frac{1}{r}\frac{dR_{2,i}}{dr}-(\lambda^2+\frac{1}{r^2})R_{2,i}=0, \quad (3.30)$$

$$\frac{d^2Z_{2,i}}{dz^2}+k^2Z_{2,i}=0, \quad (3.31)$$

where i=0, 1…..N, $\lambda^2=k^2+jP^2$ and k is a continuous variable. Considering the solution of Eq. (3.30) and Eq. (3.31) the general solution of Eq. (3.24) will be

$$A_{2,\varphi}(r,z)=\sum_{i=0}^{N}\int_{0}^{\infty}D_i(k)K_1(\lambda r)\cos k(z-ih). \quad (3.32)$$

In the above expression only the Bessel function k is used, because the vector potential due to excitation inside the material vanishes as we move away towards infinity. The solution of Eq. (3.30) and Eq. (3.31) considering that $Z_{2,i}$ is symmetrical about the i[th] loop plane is $Z_{2,i}(z)=\cos k(z-ih)$.

The magnetic vector potential $\vec{A}_1''$ in region 1 will have an expression similar in the form to Eq. (3.32), so that Eq. (3.26) will be

$$A_{1,\varphi}(r,z)=\sum_{i=0}^{N}A'_{1,\varphi}(r,z)+\sum_{i=0}^{N}\int_{0}^{\infty}C_i(k)I_1(kr)\cos(z-ih)dk \tag{3.33}$$

Applying now the boundary condition, the continuity of the tangential field intensity and the continuity of the normal flux density, we may determine the constants $C_i(k)$ and $D_i(k)$ of Eq.(3.32) and Eq.(3.33) [44]

$$C_i(k)=\frac{\mu a I I_1(ka)\left[kK_0(kb)K_1(\lambda b)-K_0(\lambda b)K_1(kb)\right]}{\pi\left[\lambda K_0(\lambda b)I_1(kb)+kI_0(kb)K_1(\lambda b)\right]}, \tag{3.34}$$

$$D_i(k)=\frac{\mu a I I_1(ka)}{\pi b\left[\lambda K_0(\lambda b)I_1(kb)+kI_0(kb)K_1(\lambda b)\right]}. \tag{3.35}$$

These constants have the value for all i**.**

Considering now the Maxwell's equation, Ohm's law and the relation:

$$\vec{B}=\vec{\nabla}\times\vec{A}. \tag{3.36}$$

The components of the magnetic field in the region 1 and 2 can be obtained as follows

$$B_{1,r}(r,z)=\sum_{i=0}^{N}\int_{0}^{\infty}kC_i(k)I_1(kr)\sin k(z-ih)dk+\frac{\mu a I}{\pi}\sum_{i=0}^{N}\int_{0}^{\infty}kI_1(ka)K_1(kr)\sin k(z-ih)dk, \tag{3.37}$$

$$B_{2,r}(r,z)=\sum_{i=0}^{N}\int_{0}^{\infty}kD_i(k)K_1(\lambda r)\sin k(z-ih)dk, \tag{3.38}$$

$$B_{1,Z}(r,z)=\sum_{i=0}^{N}\int_{0}^{\infty}C_i(k)I_0(kr)\cos k(z-ih)dk-\frac{\mu a I}{\pi}\sum_{i=0}^{N}\int_{0}^{\infty}kI_1(ka)K_0(kr)\cos k(z-ih)dk, \tag{3.39}$$

$$B_{2,Z}(r,z)=\sum_{i=0}^{N}\int_{0}^{\infty}\lambda D_i(k)K_0(\lambda r)\cos k(z-ih)dk. \tag{3.40}$$

3.4.2. Approximation of Modified Bessel function

For large values of r

$$I_n(\lambda r)=\frac{e^{\lambda r}}{\sqrt{2\pi\lambda r}}\left[1-\frac{(4n^2-1^2)}{1(8\lambda r)}\left(1-\frac{(4n^2-3^2)}{2(8\lambda r)}\left(1-\frac{(4n^2-5^2}{3(8\lambda r)}(1-\ldots)\right)\right)\right] \tag{3.41}$$

$$I_0(\lambda r)=\frac{e^{\lambda r}}{\sqrt{2\pi\lambda r}}\left[1-\frac{1}{8\lambda r}\left(1+\frac{9}{2(8\lambda r)}\left(1+\frac{25}{3(8\lambda r)}(1+\ldots)\right)\right)\right] \tag{3.42}$$

$$I_1(\lambda r)=\frac{e^{\lambda r}}{\sqrt{2\pi\lambda r}}\left[1-\frac{3}{8\lambda r}\left(1+\frac{5}{2(8\lambda r)}\left(1+\frac{21}{3(8\lambda r)}(1+\ldots)\right)\right)\right] \tag{3.43}$$

When n is a positive integer the second kind of modified Bessel function (K_n) can be written as:

$$K_n(\lambda r) = \sqrt{\frac{\pi}{2\lambda r}} e^{-\lambda r} \left[\left(1 + \frac{(4n^2 - 1^2)}{1(8\lambda r)} \left(1 + \frac{(4n^2 - 3^2)}{2(8\lambda r)} \left(1 + \frac{4n^2 - 5^2}{3(8\lambda r)} (1 + \ldots) \right) \right) \right) \right], \tag{3.44}$$

$$K_0(\lambda r) = \sqrt{\frac{\pi}{2\lambda r}} e^{-\lambda r} \left[\left(1 - \frac{1}{8(\lambda r)} \left(1 - \frac{9}{2(8\lambda r)} \left(1 - \frac{25}{3(8\lambda r)} (1 - \ldots) \right) \right) \right) \right], \tag{3.45}$$

$$K_1(\lambda r) = \sqrt{\frac{\pi}{2\lambda r}} e^{-\lambda r} \left[1 - \frac{3}{8(\lambda r)} \left(1 - \frac{5}{2(8\lambda r)} \left(1 - \frac{21}{3(8\lambda r)} (1 - \ldots) \right) \right) \right]. \tag{3.46}$$

For a fixed n, when $r \rightarrow \infty$

$$I_n(\lambda r) \propto \frac{1}{\sqrt{2\pi\lambda r}} e^{\lambda r}. \qquad \text{And} \qquad K_n(\lambda r) \propto \sqrt{\frac{\pi}{2\lambda r}} e^{-\lambda r}. \tag{3.47}$$

With Eq. (3.46) as start, we use the modified Bessel function expansion of the K_n value and specifically in region 2 $B_{2,r}(r,z)$ can be written as:

$$B_{2,r}(r,z) = \sum_{i=0}^{N} \int_0^\infty k D_i(k) \sqrt{\frac{\pi}{2\lambda r}} e^{-\lambda r} \sin k(z - ih) dk, \tag{3.48}$$

suppose $\delta = \dfrac{1}{\lambda}$,

where $\lambda^2 = k^2 + j(\mu\omega\sigma)^2$,

Where j = 1, 2, corresponds to the two regions 1, 2, respectively and i = 0, 1…..N refers to the number of the loops and also k is a continuous variable.

$$B_{2,r}(r,z) = \sum_{i=0}^{N} \int_0^\infty k D_i(k) \sqrt{\frac{\pi}{2r\left(k^2 + j(\mu\omega\sigma)^2\right)^{\frac{1}{2}}}} e^{-r\left(k^2 + j(\mu\omega\sigma)^2\right)^{\frac{1}{2}}} \sin k(z - ih) dk. \tag{3.49}$$

At origin (i.e), $z = 0$ the desired magnetic field would be mathematically written as:

$$B_{2,r}(r,0) = \sum_{i=0}^{N} \int_0^\infty D_i(k) \left(\frac{\pi}{2r(k^2 + j(\mu\omega\sigma)^2)^{\frac{1}{2}}} \right)^{\frac{1}{2}} e^{-r(k^2 + j(\mu\omega\sigma)^2)^{\frac{1}{2}}} k \sin k(-ih) dk, \tag{3.50}$$

$$B_{2,r}(r,0) = \sum_{i=0}^{N} D_i(k) \int_0^\infty \left(\frac{\pi}{2r\left(k^2 + j(\mu\omega\sigma)^2\right)^{\frac{1}{2}}} \right)^{\frac{1}{2}} e^{-r\left(k^2 + \frac{2j}{\delta^4}\right)^{\frac{1}{2}}} k \sin k(-ih) dk, \tag{3.51}$$

$$B_{2,r}(r,0)=\sum_{i=0}^{N} D_i(k)\int_0^{\infty}\left(\frac{\pi}{2r\left(k^2+j(\mu\omega\sigma)^2\right)^{\frac{1}{2}}}\right)^{\frac{1}{2}} e^{-r/\delta\left(\left(\frac{k}{\delta}\right)^2+\frac{2j}{\delta^2}\right)^{\frac{1}{2}}} k\sin k(-ih)dk, \qquad (3.52)$$

Specifically, assume that $B_{2,r}(r,0)$ field is at location ***r*** produce by direct field flowing in the coil and $B_{2,r}(r,0)$ Can be evaluate numerical for a specific results can be determine. But we can see an insight to the field profile inside the conductor by approximation some of the elaboration is treated as the follows.

$$B_{2,r}(r,0)=\exp^{-r/\delta}\left(\sum_{i=0}^{N} D_i(k)\int_0^{\infty}\left[\frac{\pi}{2r(k^2+j(\mu\omega\sigma)^2)^{\frac{1}{2}}}\right]^{\frac{1}{2}} e^{-\left(\frac{k}{\delta}+\frac{2j}{\delta^2}\right)} k\sin k(-ih)dk\right). \qquad (3.53)$$

From equation 3.53 the constant terms

$\left(\sum_{i=0}^{N} D_i(k)\int_0^{\infty}\left[\frac{\pi}{2r(k^2+j(\mu\omega\sigma)^2)^{\frac{1}{2}}}\right]^{\frac{1}{2}} e^{-\left(\frac{k}{\delta}+\frac{2j}{\delta^2}\right)} k\sin k(-ih)dk\right)$ is represented by $c(\delta)$ and finally the field equation would be approximately , $B_{2,r}(r,0)\approx c(\delta)e^{-r/\delta}$. So therefore, one can arrive the MRI signal has direct relation with magnetic field ($B_{2,r}(r,0)$) and mathematically can be expressed as the flowing:

$$Signal \propto B_{2,r}(r,0). \qquad (3.55)$$

Lastly the field equation has the flowing form:

$$B_{2,r}(r,z)=C(z,\delta)e^{-r/\delta}. \qquad (3.56)$$

The Eq. 3.56 indicates that the amplitude of magnetic field exponentially decays to 1/e of their values $r=0$ in distance and the exponential decay r causes attenuation of the EM field. For large value of radial distance there will be low signal and no image is formed. In general the results show that there is no image detected due to by B_1field is exponentially became decay. The MRI signal is directly proportional to B_1 and magnetization.

3.5 Results and Discussion

The theory in the previous section has been implemented in the FORTRAN Program software language (ubuntu 14). The $B_{2},_{r}(r,0)$ is the final result of the above analysis and the approximating of RF field is obtained by the separation of variables method. Numerical simulation was performed on a given metal coil at different relative orientations to the RF field and the skin depth effect in order to explore the geometry dependence of the field strength. Plot of the numerically B_1 field at location on the surface of the metal object in figure 3.2 show that it has a strong dependence on B_1 field. For the increasing of B_1 field there will be also high signal. Typically the order of skin depth character can limit B_1 penetration in to a metal .This in turn, results attenuated MRI signal. In case for large value of r maximum skin depth of EM field will be attenuate and mean while magnetic field will decrease due to B_1 and no signal is detected at that region. And this region is EM vacuum. The fig.3.3 below indicates that the simulation result is done interims of modi: ed Bessel function and the skin depth effects.

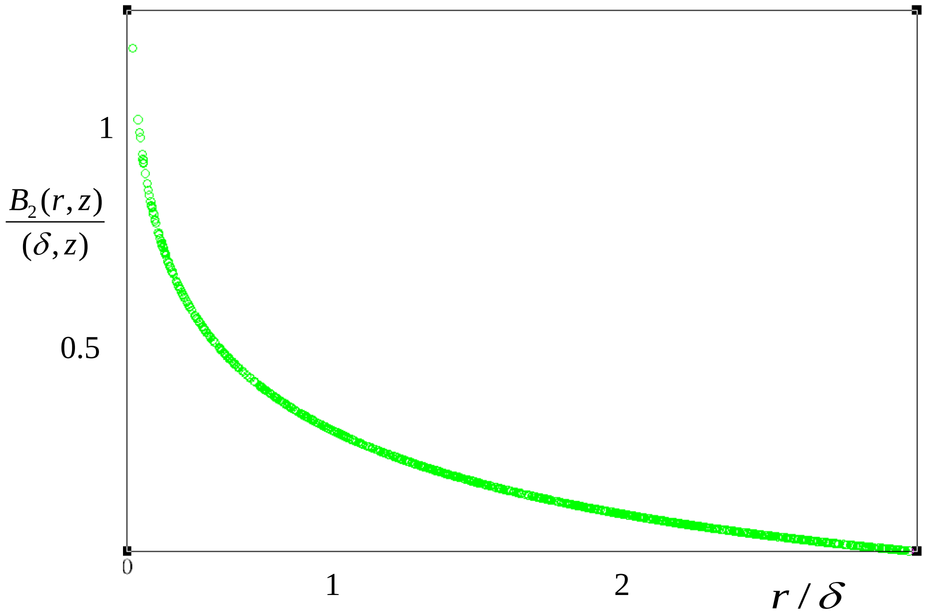

Fig.3.3. Exponential decay of magnetic field and the function of depth from the metal surface.

The $B_2(r,0)$ field strength varies as function of the distance from the surface. For minimum skin depth the $B_2(r,0)$ will limit mean while attenuated signal is detected .This leads to decreasing MRI signal. All analytic calculation involved in the evaluation of the skin depth effect and subsequent construction of $B_{2,r}(r,0)$ are exponential and modified Bessel functions accurate routines within the FORTRAN simulation for their evaluation.

Chapter Four

4. Summary and conclusion

EM fields do not propagate in conductor as freely as in vacuum or dielectrics. In fact, they encounter strong resistance when they try to penetrate in to conductor. The two most important health-related properties of the EM fields are frequency and field strength. The exaction inside shell and shell of infinite thickness, the distribution of the RF fields are described in a geometrical configuration consisting of a cylindrical shell of the infinite length and thickness. A simulation for this work is provided based on the quasi-static approximation of the Maxwell equations and EM field analysis.

The dependence of the B_1 field on the orientation of metal plate placed within the B_1coil has been investigated both analytically and numerically. This dependence was explored using analytical field calculations that have been validated by direct comparison to simulation of MRI concept. The field of the induced EM field within the material of region **2** at any point varies both the radial distance ***r*** and the axial distance ***z.*** For the solution it is assumed that the displacement current can be neglected, because of power frequency is used and the dimension of the apparatus are small compared with the corresponding wave length. For plane wave, the skin depth is the distance for which the amplitude of the magnetic field or the current density drops by a factor of e. The skin depth marks the depth below the surface of the conductor at which the current density has fallen to $1/e$ of the value at the surface. I also analytically calculate the $B_2(r,0)$ field in the sample space with introduced magnetic field orientation MRI coils. For large value ***r*** and minimum skin depth of EM field will be attenuated and also magnetic field will be decrease and no signal will detected at that region. From the result I conclude that the absence image detected in EM vacuum due to MRI signal is exponentially decay and the region is named to be EM vacuum.

REFERENCES

[1] F.Bloch ,"Nuclear induction ,"Phys Rev. vol.70.pp 460-474, 1946.

[2] E.Purcell." effects of diffusion on free precession in nuclear magnetic resonance experiments" C. Lauterbur. Image formation by induced local interactions: Examples employing NMR. *Nature*, 242:190–191, 19745

[3] Gold GE, Suh B, Sawyer-Glover A, Beaulieu C. Musculoskeletal MRI at 3.0 T: initial clinical experience. AJR Am J Roentgenol. Nov 2004; 183(5):1479-1486

[4] P.Mansfield," Multi-planar image formation using NMR spin choes ".J.Phys.C; Solid state Phys .vol.10,pp 55-58 .1977.

[5] Isidor I. Rabi (Nobel Prize in Physics, 1944) "NMR phenomenon in molecular beams''1937.

[6] Genuis, S.J. Fielding a current idea: Exploring the public health impact of electromagnetic radiation. *Public Health* 2008, *122*, 113–124

[7]. S.S. Hidalgo-Tobon, "Theory of Gradient Coil Design Methods for Magnetic Resonance Imaging", *Concepts Magnetic Resonance*, pp. 223-242, 2001.

[8] P. Robitaille andL. Berliner, *Ultra High Field Magnetic Resonance Imaging*, Springer, New York, 2006.

[9] J. Jin, Electromagnetic Analysis and Design in Magnetic Resonance Imaging, CRC Press LLC, Florida, 1999.

[10] R. Klucznik, D. Carrier, R. Pyka, R. Haid, Placement of aferromagnetic intracerebral aneurysm clip in a magnetic field with afatal outcome, Radiology 187 (1993) 855–856.

[11] J.A. Patton, MR imaging instrumentation and image artifacts, Radio graphics 14 (1994) 1083- 1096.

[12] J.A. Malko, J.C. Hoffman Jr., P.J. Jarrett, Eddy-current-induced artifacts caused by an ''MR-compatible'' halo device, Radiology 173 (1989) 563–564

[13] H. Graf. G. Steidle, P. Martirosian, U.A. Lauer, F. Schick, Effects on MRI due to altered RF Polarization near conductive implants or instruments. Med. Phys. 33 (2006) 124-127.

[14] K. El Banan, W. Handler, B. Chronik, S.P. Salisbury, Heating of metallic rods induced by time varying gradient field in MRI, J. Magn. Reson. Imaging 38 (2013) 411-416

[15] H. Graf, G. Steidle, U.A. Lauer, F. Schick, RF enhancement and shielding in MRI caused by conductive implants: dependence on electrical parameters for a tube model, Med. Phys. 32 (2005) 337-342

[16] C. M. Collins, “Numerical field calculations considering the human subject for engineering and safety assurance inMRI,” *NMR Biomed.*, vol. 22, no. 9, pp. 919–926, 2009.

[17] M A Bernstein, K F King and X J Zhou, *Handbook of MRI Pulse Sequences*, Elsevier Academic Press, San Diego, 2004

[18] I. I. Rabi, J. R. Zacharias, S. Millman, and P. Kusch. A New Method of Measuring Nuclear Magnetic Moment. Physical Review, 53(4), 318, (1938).

[19] D. R. Bailes and D. J. Bryant. NMR imaging. *Contemporary Physics*, 25:441, 1984.

[20] M. Haacke, R.W. Brown, M. R. Thompson, R. Venkatesan, M RI: Physical Principles and Sequence Design, Wiley-Liss, New York, (1999), 47 - 71

[21] E.Mark Haacke, Robert W. Brown, Michael R. Thompson. Magnetic Resonance Imaging and sequence design. AJ. Wiley and Sons, Inc, New York, 1999.

[22] Jorge Jovicich, Basic Principles of Magnetic Resonance, (2001),2-10

[23] M. Elumalai, “Birdcage Coils for MRI-in Vivo Imaging of 25-Chlorine and 1-Hydrogen Nuclei,” *Magnetic Resonance Imaging*, pp. 1-16, 2011

[24] M. Lang, “Building a Birdcage Resonator for Magnetic Resonance Imaging Studies for CNS Disorders,” University of Winnipeg, April 2011.

[25] UIUC Physics 436 EM Fields and Sources II lecture notes of EM wave propagation in conductor.

[26] JMRI – J. Magn. Reson. Imaging 5 (1995) 75– 88. C.R. Camacho, D.B. Plewes, R.M. Henkelman, Nonsusceptibility artifacts due to metallic objects in MR-imaging.

[27] A.J. Ilotta, S. Chandrashekar, A. Klöcknerc, H.J. Chang, N.M. Trease, C.P. Grey, L. Greengard, A. Jerschow, Visualizing skin effects in conductors with MRI: 7Li MRI experiments and calculations, J. Magn. Reson. 245 (2014) 143–149.

[28] A.J. Ilotta, S. Chandrashekar, A. Klöcknerc, H.J. Chang, N.M. Trease, C.P. Grey, L. Greengard, A. Jerschow, Visualizing skin effects in conductors with MRI: 7Li MRI experiments and calculations, J. Magn. Reson. 245 (2014) 143–149.

[29] Bhattacharyya, R. et al. In situ NMR observation of the formation of metallic lithium microstructures in lithium batteries. Nature Mater. 9, 504-510 (2010).

[30] J. D. Jackson, Classical Electrodynamics. New York: John Wiley & Sons Inc., 1999 3.

[31]. Lorrainp and Corson, D., 1970, *Electromagnetic Fields and waves*, 2nd edn (San Francisco: W. H. Freeman).

[32] Fawwaz T. Ulaby. Fundamentals of Applied Electromagnetics. (1997), 2001 media edition, PrenticeHall Inc., Upper Saddle River, New Jersey, 07458, USA.

[33] Ernst RR, Anderson WA. Applications of Fourier transform spectroscopy to magnetic resonance. Rev Sci Instrum 1966; 37:93–102.

[34] Rangeet Bhattacharyya, Baris Key, Hailong Chen, Adam S. Best, Anthony F. Hollenkamp, Clare P. Grey. In situ NMR observation of the formation of metallic lithium microstructures in lithium batteries. Nature Materials, (2010), 9, 504510

[35] C. A. Balanis, Advanced Engineering Electromagnetics. Reading Massachusetts Addison Wesley, Inc. USA, 1989.

[36] E. Fukushima, S.B.W. Roeder, Experimental pulse NMR, Addison- Wesley, Massachusetts, USA, 1981.

[37] J. D. Jackson, *Classical Electrodynamics*. New York: John Wiley & Sons Inc., 1999.

[38] W. A. Edelstein, T. K. Kidane, V. Taracila, T. N. Baig, T. P. Eagan, Y. N. Cheng, R. W. Brown, and J. A. Mallick, *Active-passive gradient shielding for MRI acoustic noise reduction*, Magnetic Resonance in Medicine 53:1013-1017, 2005.

[39] LORRAINPand CORSON, D., 1970, *Electromagnetic Fields and Waves*, 2nd edn (San Francisco: W. H. Freeman).

[40] MINISTRY of TECHNOLOGY 1968, *Intense Radio Frequency Radiation Code of PracticMOT* Report BR 19945 (H.M.S.O.).

[41] JOHNSON, C. C., and GUY, **A.** W., 1972**,** *Proc. IEEE, 60***,** 692-718.

[42] SCHELEUNOFSF., A., 1943, *Electromagnetic Waves* (New York**:** Van Nostrand).

[43] SPIEGEL, M. R., 1968, *Mathematical Handbook of Formulas and Tables* (New York: McGraw-Hill).

[44] Tegopoulos J.A ,1924 “Eddy currents in linear conducting media” studies in electrical and electronic engineering ,New York ,NY(vol.16)

[45] J.A Tegopoulos P.P.Yanopoulos “Eddy current and loss in cylindrical structures due to circular currents part I. Hollow cylinder” IEEM conference paper G214,1978.

[46] J. A. Tegopoulos and E. E. Kriezis, "Eddy Current Distribution in Cylindrical Shells of Infinite Length Due to Axial Currents, Part II: Shells of Finite Thickness". Paper: 70 TP 600-PWR.

[47] N. W. McLachlan. Bessel functions for Engineers. Oxford University Press, London, England, Second Edition, 1955.